Free-Radical Kinetics at High Pressure: A Mathematical Analysis of the Flow Reactor

Neil M. Donahue,* James S. Clarke, Kenneth L. Demerjian,† and James G. Anderson

Department of Chemistry, Harvard University, Cambridge, Massachusetts 02138

Received: August 30, 1995; In Final Form: January 4, 1996[⊗]

Highly accurate reaction rate constants may be extracted from data obtained in well-developed (laminar or turbulent) diffusive flow over a wide range of experimental conditions. In many cases, data obtained in the core of such a flow may be treated as if the flow were one dimensional, leaving only a small correction for radial diffusion. This correction factor is derived analytically and presented in terms of easily observed quantities. The correction is robust; experimental and theoretical evidence is presented showing that it is insensitive to assumed axial symmetry and remains small so long as the interaction between the core and wall of a flowtube falls within well-defined bounds. The major limitations to accuracy in our high-pressure flow kinetics system (HPFS) are discussed in conjunction with observations of bimolecular reaction rate constants made over a very wide range of experimental conditions for the reactions OH + ethane → products and OH + cyclohexane → products. In the current experiment, accuracy for hydroxyl radical reactions is limited to roughly 12% for pressures of nitrogen ranging from 2 to 600 Torr. The accuracy in the measured ratio of two hydroxyl radical reaction rate constants is roughly 6%. Accuracy is currently limited primarily by absolute velocity measurements and by radical detection sensitivity. Strategies for further improving the accuracy of the high-pressure flow (HPF) technique are discussed.

Introduction

Recent analyses of stratospheric chemical observations (Cohen et al. [1994], Wennberg et al. [1994b]) have demonstrated the urgent need for highly accurate kinetic data in order to extract mechanistic conclusions from in situ observations. The need is especially acute for radical−molecule reactions at the low temperatures (190−250 K) and moderate pressures (20−200 Torr) encountered in the upper troposphere and lower stratosphere. In many cases, changes to critical rate constants of 10% at 200 K and 50−150 Torr (6.5−19.5 kPa) significantly alter the agreement between observations and models; this level of accuracy is seldom quoted in reviews (i.e., JPL [1994], Atkinson et al. [1991]), even at room temperature. Extrapolation of kinetic observations from elevated temperatures and either elevated or reduced pressures is perilous, as reduced temperatures expose subtle details of the electronic potential energy surface, resulting in sensitive functional dependence on both pressure and temperature.

Figure 1 depicts the types of potential energy surfaces frequently encountered in radical molecule reactions, ranging from (I), a pure bond association−dissociation surface with no identifiable saddle point, to (VI), a pure atom abstraction surface with a simple barrier. In this rendition, the curvature of the surface at each transition state depicts the relative tightness or looseness of the state, with tight states being constrained entropically. The evolution from one surface to the other is mathematically straightforward. It even represents something of a continuum in quantum-mechanical theory, as the repulsive wall in surface (I) develops an exit channel with a tight transition state (TS#2) of ever decreasing energy, while a relatively loose transition state (TS#1) of ever increasing energy develops in the entrance channel. The first transition state is generally governed by long-range (van der Waals) and frontier orbital (HOMO−LUMO) interactions, whereas the second transition state must be governed by the interaction between the LUMO of the radical and the reactive molecular orbital (RMO) in the molecule (Toohey and Anderson [1989]). In the event that the HOMO and RMO are identical, simple bimolecular behavior may result; however, if the HOMO and RMO are different, complex formation is likely (Dubey [1994]).

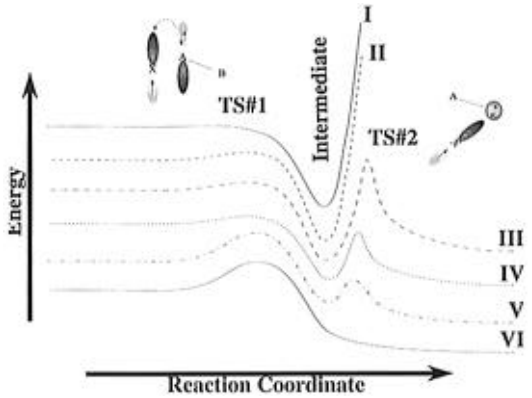

Figure 1. Evolution from unimolecular to bimolecular reactions. Reactions range from unimolecular reactions where a single, stable adduct is formed or broken (type I) to bimolecular reactions, which proceed over a simple barrier (type VI). In between are reactions with multiple transition states with varying energies and entropies; both profoundly affect the observed rate constant.

The effect of these various surfaces on the overall rate constant, expressed as a function of pressure and temperature, is anything but straightforward. Potential energy surfaces of type I (i.e., O + O → O_2, Tsang and Hampson [1986]) exhibit a pressure dependence well described by RRKM theory (Troe [1980]), with a small negative temperature dependence (increasing rate with decreasing temperature). Likewise, potential energy surfaces of type VI (i.e., OH + CH_4 → H_2O + CH_3, Atkinson [1991]) exhibit simple Arrhenius behavior with no pressure dependence, but the transition from one to the other is not monotonic. Surfaces like III (i.e., OH + NH_3 → H_2O + NH_2, Dubey [1994]) and V (i.e., O + ClOCl → ClO + ClO, Stevens and Anderson [1992]) may appear to have purely Arrhenius traits at elevated temperatures and low pressures, only

† Also at Atmospheric Sciences Research Center, State University of New York, Albany, New York.

⊗ Abstract published in *Advance ACS Abstracts,* March 1, 1996.

0022-3654/96/20100-5821$12.00/0

to display unusual behavior as temperatures drop and pressures rise; they may also exhibit depressed *A* factors under all conditions. Surfaces of the middle type, type IV (i.e., OH + $HONO_2 \rightarrow H_2O + NO_3$, Dubey [1994]) can be more or less "normal", or exhibit strongly negative temperature dependencies and very low *A* factors, along with moderate pressure dependencies, as the overall rate constant is determined by subtle details of the competition at the reactive intermediate among dissociation into products, dissociation into reactants, and stabilization.

For this reason, we have been developing methods to accurately measure radical molecule rate constants over the entire range of atmospheric conditions. In this paper we shall focus on aspects of this design effort that constrain the accuracy of our measurements at room temperature over a very wide range of pressures. Future work will explore the methods below and above ambient temperatures.

High-pressure flow (HPF) kinetics depends on a tractable separation of fluid dynamics and chemistry in a kinetics flow system. Unlike low-pressure discharge flow kinetics (Howard [1979], Kaufman [1984]), which relies on rapid radial diffusion to produce a straightforward relation ($d = \bar{v}t$) between axial position, bulk flow velocity, and reaction time, HPF kinetics confronts the full continuity equation head on. Abbatt et al. [1990] (hereafter A90) advanced the HPF technique to nearly full maturity by extending the work of Keyser [1984] with several critical additions: a larger diameter reaction zone was used, and the radicals under study were confined to the core of the carrier gas flow, allowing the entire reaction to occur before diffusion to the wall significantly contributed to the radical plume shape; multiple radical detectors were employed, removing the need for moving or multiple injectors; and turbulent flow was treated in addition to laminar flow, allowing a far greater range of pressures to be explored. Most importantly, very few assumptions were made about the fluid dynamics of the system. Important advances in high-pressure turbulent flow (Westbrook et al. [1977], Seeley et al. [1993]) have generally been tied to creating effective plug flow conditions in turbulence (well mixed reagents in a bulk flow). The conditions favored by A90 were the opposite of plug flow: in place of rapid radial diffusion they initiated reactions in conditions where radial diffusion was slow compared to characteristic reaction times and then explicitly treated the coupled diffusion and kinetic equations to obtain the desired rate constant.

It was a surprising experimental observation in A90 that data from their HPF system could be analyzed in a manner very similar to traditional discharge flow systems, with the core velocity replacing the bulk velocity in the simple $d = vt$ relation, a finding quite different from Keyser [1984]. This result applied to all conditions investigated in A90, under both turbulent and laminar flow, from 7 to 400 Torr. Specifically, A90 verified that rate constants could indeed be derived by carefully mapping out the first and second derivatives of a two-dimensional radical plume evolving in fully developed axial flow and then solving the continuity equation for both the diffusion constant and the desired chemical rate constants. They also found, however, that the same rate constant could be determined with much greater precision by confining radical measurements to the spine of the radial plume and analyzing the data in the traditional manner, finding the rate of change of the slope of the spine of the radical plume with respect to excess reagent concentration. Because of its ease and high precision, this second method was adopted as the primary method for HPF data analysis, though no theoretical assessment of the method or its accompanying errors was presented.

The implications of "anti plug flow" kinetics are far reaching. Where traditional, low pressure, discharge flow measurements were confined to pressures of a few Torr, the upper pressure bound to HPF kinetics is imposed by radical quenching; using the system developed by A90, we have measured hydroxyl radical reactions above 600 Torr (Donahue et al. [1995a]), an increase of 2 orders of magnitude in density. Where the wall was an integral part of low-pressure discharge flow systems, it is now absent. Diffusion times from the core to the wall of our HPF system are generally on the order of 1 s, while experiments cover 0.1 s of reaction time. Radicals measured in the core of the flow thus have no contact with the wall through the reaction zone. This greatly expands the temperature range open to the system, as wall-catalyzed reactions can be avoided at low temperatures. Finally, the system involves very few assumptions about fluid dynamics; by using well-developed turbulent or laminar flow under conditions of slow mixing, the influences of fluid dynamics may be factored out with high accuracy.

The purpose of this paper is to provide a theoretical fundament for high-pressure flow kinetics, grounding the simple data analysis procedure of A90 while developing a small correction factor for the effects of radial diffusion on the observed rate constant. This correction explains spurious pressure dependencies observed on the HPF system in purely bimolecular reactions. The motivation is the demonstrated need for very accurate kinetics data to augment in situ atmospheric observations for atmospheric chemistry research. We shall examine the limits to both precision and accuracy of hydroxyl radical kinetics in the HPF system, focusing on approaches which reduce to a minimum the number of parameters that must be accurately known and discussing ways in which both experimental precision and accuracy may be improved.

Theoretical Considerations

Experimental Concept. We shall first consider an ideal flow system in which diffusion corrections are absent. This will allow us to develop the basic equations of high-pressure flow kinetics, as well as to examine the methods of data analysis. Most of the sources of error contributing to the overall accuracy of our measurements will surface in this discussion. The extent to which neglecting diffusion fails to explain our data will motivate the subsequent treatment of diffusion.

Motivation. We consider kinetic observations conducted in a well-established flow of some carrier gas. An idealized experiment is depicted in Figure 2. The flow is assumed to be fully laminar or fully turbulent, with a velocity profile ($V(r)$) a function of radius only. Temperature and pressure are assumed to be constant. The carrier gas contains a well-mixed but slowly varying concentration of an "excess" reagent, XS, whose concentration is assumed to be independent of both radial and axial position. At some location, radicals are added to the center of this flow in such a way as to neither disturb the flow nor create a long-lasting inhomogeneity in the reagent concentration. These radicals form a plume ($C(r,z)$) whose steady state shape is governed by the balance of four major terms in the continuity equation: net axial advection, radial diffusion, axial diffusion, and first-order chemical loss ($k^1 = k[\mathrm{XS}]$). The plume is assumed to be roughly Gaussian in shape, with unspecified (but probably high) radical loss at the wall. For a given point along the spine of the plume, the axial terms (advection and diffusion) act as sources, while the radial diffusion and first-order chemical loss terms act as sinks.

The effect of adding excess reagent to this flow is depicted in the two panels of Figure 2. With low [XS] and sufficiently

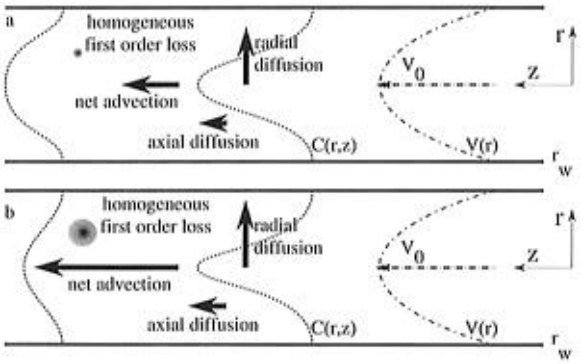

Figure 2. Continuity equation in a flow system. A well-developed velocity profile, $V(r)$, advects a radical plume, $C(r,z)$, in the presence of diffusion and first-order chemistry (k[XS]). The velocity profile is shown as a dashed parabola. The radical plume is shown as a dotted broadening Gaussian at two axial positions. The terms in the continuity equation are depicted graphically for the core of the flow. Net advection is a large source. Axial diffusion is a small source. Radial diffusion is a large sink. First-order chemical loss, assumed to be homogeneous, is a net sink of varying size. (a) Low first-order loss: diffusion balances net advection. (b) High first-order loss: first-order chemical loss greatly steepens the axial concentration gradient, increasing net advection to maintain the steady state; diffusion is slightly increased.

high velocity, radial diffusion, and net advection balance, with little contribution from either axial diffusion or chemical loss. As [XS] (and thus the first-order loss term) increases, so does the axial concentration gradient; this in turn causes the net advection term to increase to balance the loss term. In addition, the plume tends to become sharper, causing more radial diffusion, while the axial diffusion term also grows.

Traditionally, discharge flow kinetics has been carried out under conditions where the radial diffusion term is extremely rapid, which allows the continuity equation to be integrated over the radius of the tube. Provided that wall losses and axial diffusion are kept tolerably small, the continuity equation reduces to a simple balance between the first-order chemical loss term and the radially averaged advection term, with time equal to the quotient of axial distance and average velocity. This is the plug flow approximation (Howard [1979]). A second option is to measure the velocity profile and the radical plume (as a function of radius and axial position) and to invert the full continuity equation. This is one of the approaches used by A90. Finally, one may focus solely on the spine of the radial plume, at $r = 0$, treating each term with the attention required by its influence on the rate constant inversion. This approach was shown by A90 to yield results indistinguishable from the full continuity equation inversion, despite the counterintuitive assumption that the effects of diffusion could be entirely neglected. This approach, along with its assumptions, is the main subject of this paper.

Chemical Equations. Downstream of the radical injection point, after the reagent has thoroughly mixed into the spreading radical plume, the radicals are observed at several locations, or detection axes, which together constitute the reaction zone. For the reaction between a radical with concentration C and XS, in a Lagrangian frame of reference with no diffusion, we have

$$\frac{\mathrm{d} \ln C}{\mathrm{d}t} = -k[\mathrm{XS}] \tag{1}$$

We can assume a simple relationship between axial distance, z, and reaction time t: $\bar{v}$ is the average velocity of measured radicals as they flow through the reaction zone.

$$z = \bar{v}t \tag{2}$$

We may then trivially write down the standard equation for flow kinetics:

$$k = -\bar{v}\frac{\partial^2 \ln C}{\partial z\, \partial[\mathrm{XS}]} \tag{3}$$

In standard discharge flow kinetics, $\bar{v}$ is replaced with the bulk velocity, as the well-mixed radicals sample the entire velocity profile by rapidly diffusing over the entire radial extent of the flow tube. In high-pressure flow kinetics, we instead assume that radial diffusion is very slow, in which case $\bar{v}$ is replaced with $v(0)$, the velocity in the center of the flow. We also increase the precision of our measurement by performing the derivative with respect to [XS] before the derivative with respect to z, as this removes the influence of radial diffusion more rapidly from the data and also eliminates any need for intercalibration of the radical detection axes.

The surprising result of high-pressure flow kinetics is that the appropriate $\bar{v}$ remains very close to $v(0)$ even as an initially sharp radical plume disperses most of the way to the reactor wall in the reaction zone. The model presented in this paper is essentially a model of $\bar{v}$, though the details of the fluid dynamics obscure this somewhat.

Radical Measurement. We next anticipate a fluorescence radical measurement at several fixed axes. At each axis the fluorescence signal will be

$$S(C,z,t_{\mathrm{lab}}) = p(z,t_{\mathrm{lab}})\sigma\, o(z,t_{\mathrm{lab}})Q([\mathrm{XS}],t_{\mathrm{lab}})\Omega(z)\epsilon(z)C(z,[\mathrm{XS}],t_{\mathrm{lab}}) \tag{4}$$

where z indicates the position of a given axis, t_{lab} represents lab time, $p(z,t_{\mathrm{lab}})$ is the photon flux (laser power), σ is the cross section of the radical, weighted for the spectral distribution of p at optimal alignment, $o(z,t_{\mathrm{lab}})$ is the overlap between p and σ, $Q(t_{\mathrm{lab}})$ is a quenching term, $\Omega(z)$ is the detector solid angle, and $\epsilon(z)$ is the optical efficiency of each detector.

Our objective is to eliminate all terms that either drift or require absolute calibration. If we divide the signal observed at a position z by one observed at a position arbitrarily designated $z = i$, we remove two important terms: the weighted cross section and the quenching term. The power and overlap terms must be addressed next. For a laser-induced fluorescence (LIF) radical measurement, a single laser beam is passed sequentially through the several fluorescence axes. In this case $p(z,t_{\mathrm{lab}})o(z,t_{\mathrm{lab}}) = a(z)p(t_{\mathrm{lab}})o(t_{\mathrm{lab}})$, where $a(z)$ represents the laser efficiency of a particular axis (number of laser passes, if it is multipassed, optical losses between the axis and the power measurement location, etc), which is assumed to be stable. Thus

$$\frac{S(C,z,t_{\mathrm{lab}})}{S(C,i,t_{\mathrm{lab}})} = \frac{a(z)\ \Omega(z)\ \epsilon(z)C(z,[\mathrm{XS}],t_{\mathrm{lab}})}{a(i)\ \Omega(i)\ \epsilon(i)\ C(i,[\mathrm{XS}],t_{\mathrm{lab}})} \tag{5}$$

The residual calibration terms vary from axis to axis; however, a derivative of the log of S with respect to [XS] at a fixed location is performed first in the above experimental method. This eliminates these residual calibration terms from eq 5.

Excess Reagent Measurement. Finally, we must measure the excess reagent concentration. Our approach is to use a long path absorption measurement, either in the UV or the IR. In some cases a passive tracer is used to boost the absorption signal; the reagent and tracer are premixed in a sample bulb to a ratio $\zeta = [\mathrm{XS}]/[\mathrm{tracer}]$. The concentration of reagent in the HPF system at a given time is thus

$$[\mathrm{XS}] = \zeta\tau/\sigma l \tag{6}$$

where τ is the measured optical depth, l is the path length, and σ is the appropriate cross section. For direct reagent measurement $\zeta = 1$.

Expressions for the Rate Constant. We are left with the ultimate expression for deriving the experimental rate constant:

$$k = -v\frac{\sigma l}{\zeta}\frac{\partial^2}{\partial z\,\partial \tau}\ln\frac{S(z)}{S(i)} \tag{7}$$

The accuracy of this expression depends on five factors: (1) the validity of the simplifying assumption that the fluid dynamics (diffusion) is unaffected by the presence of reagent, (2) the absence of complicating chemistry above that described by eq 1, (3) the absence of uncorrected experimental drifts on the time scale of the experiment, (4) the accuracy of reagent concentration measurements, and (5) the accuracy of velocity measurements. Only the first of these five factors results in an unavoidable correction term to eq 7; the rest require careful experimental procedure and measurement. Experience has shown that system conditions (velocity profile, pressure, temperature, and general radical source characteristics) are highly stable. This allows several different reactions to be run sequentially under identical flow conditions. We can derive an expression for the ratio of two rate constants that is free of many of the sources of error in eq 7:

$$\frac{k_1}{k_2} = \frac{\sigma_1\zeta_2}{\sigma_2\zeta_1}\frac{\overline{\partial/\partial\tau\,\ln(S_1(z)/S_1(i))}}{\partial/\partial\tau\,\ln(S_2(z)/S_2(i))} \tag{8}$$

where the bar indicates averaging over the four downstream axes. In general, either the two ζ's will be unity, in which case the ratio of cross sections must be known, or the cross sections will be identical (the same tracer) and the mixing fractions will need to be accurately known. Many of systematic effects of the fluid dynamics will be eliminated by this ratio, including the effect of diffusion and any calibration uncertainty in the velocity measurement, provided that the two measurements are made under identical experimental conditions and near enough in time to prevent important drifts. In some cases systematic effects caused by secondary chemical reactions will also largely cancel. Therefore, the ratio in eq 8 will be substantially more accurate than the absolute rate described by eq 7.

We shall always report both individual absolute rate constant measurements and these ratios, generally with respect to the well-studied reaction

$$\mathrm{OH} + \mathrm{ethane} \rightarrow \mathrm{products}$$

It must be noted that this relative measurement is subject to very different sources of error from those relative rate measurements based on the long-term monitoring of disappearance rates for several reagents simultaneously exposed to a radical in a reaction chamber. We provide a direct measurement of these ratios, unambiguously related to the common radical. In many cases, interpretation of data requires accurate knowledge of these ratios, as opposed to accurate knowledge of the absolute rate constants themselves. These cases include the study of planetary atmospheres and the study of combustion chemistry. Furthermore, the higher precision of these ratios will in general greatly improve our ability to analyze pressure and temperature-dependent rate data.

Analytic Treatment of Diffusion in Flow Systems. We now turn our attention to an analytic treatement of the core of a reactive flow, focusing on the development of small correction terms to the basic data analysis method already presented. Our approach will be to present series expansion solutions to the continuity equation appropriate to a roughly Gaussian plume spreading from a point source in well-developed laminar or turbulent pipe flow. Before presenting the solutions, we will manipulate the continuity equation itself, anticipating both the rough plume shapes and the impending derivatives with respect to time and excess reagent concentration. The derivative with respect to excess reagent concentration will prove to be particularly potent, removing many of the terms in our solutions. The major assumptions in this manipulation will be that the system is azimuthally symmetric and that the contribution of the wall to the radical plume shape may be neglected. Both of these assumptions will be validated: the first by data collected in intentionally asymmetric conditions, and the second by showing that small radial diffusion corrections are equivalent to small wall contributions.

With the continuity equation in the appropriate form, we will treat first axial and then radial diffusion. We will show that axial diffusion is insignificant in our system and that the effect of radial diffusion is tolerably small under laminar conditions, ranging from 30% at 1 Torr system pressure to 3% at 20 Torr. We will derive an expression relating this radial diffusion effect to the easily measured pressure head, allowing for accurate removal of its influence. Finally, we will show that a turbulent flow profile well removed from the wall of a tube may be treated as if it were a laminar profile in an even wider tube. The result will be an equally simple correction for radial diffusion in turbulent flow that is in all cases very small, never exceeding 4% in our system.

Statement of the Problem. We shall consider the problem depicted graphically in Figure 2. Our objective is to explore the behavior of solutions to this problem under a very wide range of pressures (Reynolds numbers), developing a correction factor to eq 7 that expresses the effects of diffusion on the observed rate constant. To place the problem in context, we shall consider a system similar to our current high-pressure flow system. For this system, $v_0 \approx 10$ m/s, $k^{\mathrm{I}} \approx 0-100$/s, $D \approx 30-200$ cm^2/s, and $r_w = 6.18$ cm. The distance from the radical injector to axis 1 is 50 cm, while the spacing between each axis is 18.4 cm. We take the molecular diffusion constant of the radical to be 200 cm^2 s^{-1} Torr, consistent with the hydroxyl radical in nitrogen.

It is possible to reason through the problem in the following manner (depicted in Figure 2): A radical plume discharged into the center of the flow at the radical source will expand due to radial diffusion as it is advected downstream. Where the velocity is low or the axial curvature of the plume is very large, axial diffusion will also contribute to the propagation of the plume. As reagent is added to the system, the plume will steepen exponentially in the axial direction; this steepening will be the strongest signature of kinetics in the plume. Axial diffusion will reduce this effect, but the reduction will be small for sufficiently rapid flow. If the velocity profile is peaked, added reagent will also tend to sharpen the radical plume radially, enhancing radial diffusion. This radial sharpening will be the leading correction term to a simple advective−kinetic balance in most cases.

Continuity Equation Setup. The continuity equation for first-order chemical loss in diffusive, azimuthally symmetric pipe flow is

$$\partial C(r,z)/\partial t = -k[\mathrm{XS}]C(r,z) - \mathbf{v}(r)\cdot\nabla C(r,z) + \nabla\cdot D(r)\nabla C(r,z) \tag{9}$$

Assuming a steady state, dividing through by C, and expanding the differential operators, we obtain

$$v\frac{\partial}{\partial z}\ln C = -k[\mathrm{XS}] + \frac{D}{C}\frac{\partial^2 C}{\partial z^2} + \frac{1}{C}\frac{D}{r}\frac{\partial C}{\partial r} + \frac{1}{C}\frac{\partial D}{\partial r}\frac{\partial C}{\partial r} + \frac{D}{C}\frac{\partial^2 C}{\partial r^2} \quad (10)$$

This can be further simplified with the relation

$$\frac{\partial^2 \ln C}{\partial x^2} = \frac{1}{C}\frac{\partial^2 C}{\partial x^2} - \frac{1}{C^2}\left(\frac{\partial C}{\partial x}\right)^2 \quad (11)$$

giving

$$\underbrace{v\frac{\partial \gamma}{\partial z}}_{\text{advection}} = \underbrace{-k^{\mathrm{I}}}_{\text{first-order loss}} + \underbrace{D\left(\frac{\partial^2 \gamma}{\partial z^2} + \left(\frac{\partial \gamma}{\partial z}\right)^2\right)}_{\text{axial diffusion}} + \underbrace{\left(\frac{D}{r} + \frac{\partial D}{\partial r}\right)\frac{\partial \gamma}{\partial r} + D\left(\frac{\partial^2 \gamma}{\partial r^2} + \left(\frac{\partial \gamma}{\partial r}\right)^2\right)}_{\text{radial diffusion}} \quad (12)$$

where $k^{\mathrm{I}} = k[\mathrm{XS}]$, and $\gamma = \ln C$, anticipating the exponential nature of the solution. The collected terms correspond to the effects depicted graphically in Figure 2.

An essential technique in a kinetics experiment is to vary the excess reagent concentration ([XS]) over a wide range, thus taking a derivative with respect to [XS]. Because [XS] is assumed to be independent of position (as discussed earlier), we can carry the [XS] derivative through the axial derivative in eq 12, giving

$$k_{\mathrm{e}} = -v\frac{\partial}{\partial z}\frac{\partial \gamma}{\partial [\mathrm{XS}]} = k - \frac{\partial}{\partial [\mathrm{XS}]}(\text{diffusion}) \quad (13)$$

The thesis under examination here is that, along the spine of a radical plume (at $r = 0$), k_{e}, which corresponds to the observations in a flow system, is nearly exactly balanced by k, leaving only a small correction due to changes in the diffusion terms as [XS] changes. This is equivalent to saying that the radical plume remains geometrically similar as [XS] varies over a wide range. We shall thus refer to the term $-v(\partial/\partial z)(\partial\gamma/\partial[\mathrm{XS}])$ as the "effective reaction rate constant", k_{e}, and contributions from the diffusion terms as "corrections to the effective reaction rate constant". We must now assess the size of those corrections.

Axial Diffusion. Before considering any details of the velocity profile, we shall eliminate axial diffusion from the problem. Assuming that the radical concentration profile evolves as follows, consistent with our earlier discussion

$$C(z) \sim C_0 \mathrm{e}^{-k^{\mathrm{I}}z/v} \quad (14)$$

eq 12 becomes

$$v\frac{\partial \gamma}{\partial z} = -k^{\mathrm{I}} + \frac{Dk^{\mathrm{I}^2}}{v^2} + (\text{radial diffusion}) = -k^{\mathrm{I}}\left(1 - \frac{Dk^{\mathrm{I}}}{v^2}\right) + (\text{radial diffusion}) \quad (15)$$

This will be recognized as the axial diffusion correction used in low-pressure discharge flow kinetics (Howard [1979]). Whereas low-pressure discharge flow kinetics is frequently carried out a pressures below 1 Torr in light carrier gases, such as helium, 1 Torr is the lowest operational pressure in our system, and diffusion constants in nitrogen are relatively small. Therefore, we can consider a worst case scenario as follows: At 1 Torr, with $D \approx 200$ cm^2 s^{-1}, $k^{\mathrm{I}} \approx 100$ s^{-1}, and $v \approx 10^3$ cm s^{-1}, axial diffusion will cause a 2% error if left uncorrected. While this small correction should be applied to data taken at low pressures (and especially in light carrier gases such as He), we shall neglect it for the remainder of this discussion.

Dimensional Analysis of Radial Diffusion. Drawing on the idea of an average velocity presented earlier, we can use dimensional arguments to predict the form and rough magnitude of the radial diffusion correction. We consider a flow with center velocity, v_0, a diffusion constant, D, and an effective radius, r_{e}, such that the velocity profile in the core of the flow is $v = v_0(1 - r^2/r_{\mathrm{e}}^2)$. The time to travel a distance z will be $t = z/v$. In this time, the radical in the core will diffuse an average distance $\rho = \sqrt{Dt}$. If we assume that the average velocity of the radical is equal to the velocity at this average diffusional radius, we find

$$\langle v \rangle = v_0\left(1 - \frac{Dz}{r_{\mathrm{e}}^2 v_0}\right) \quad (16)$$

Note that the correction increases with increasing distance from the absolute origin of the plume. This is the first indication that we will want to perform kinetics experiments with sharp plumes, which is somewhat counterintuitive.

At very low pressures (high diffusion), long advection distance, or small radius, diffusion to the wall is rapid, and the appropriate average radial velocity is the bulk velocity, $^1/_2 v_0$; this is the velocity used in low-pressure discharge flow studies (Howard [1979]). The size of the correction factor in eq 16 is thus also a measure of the effect of the tube wall; as it approaches $^1/_2$, the influence of the wall becomes large. The correction factor is small at high pressures (low diffusion), short distance, or large effective radius, and the appropriate average radical velocity is thus the uncorrected core velocity. Note that we can generally treat turbulence by assuming that it increases the effective radius of the tube; a turbulent profile will thus lead to a small velocity correction.

In all cases, we expect the radial diffusion correction to be less than 1; uncorrected data will tend to give reaction rate constants that are somewhat too large. This can be easily understood, as chemistry will tend to sharpen the radical plume, thus increasing the radial curvature and so increasing the loss rate out of the core.

Flat Velocity Profile. Returning to the continuity equation, we shall first consider a nonphysical situation in which the velocity is a constant. This situation approximates that in which the radius of curvature of the velocity profile is very large. In light of our earlier discussion, we expect any radial diffusion correction to the effective reaction rate constant to be very small in this case. However, the solutions to the continuity equation will serve as the building blocks for solutions in more complicated situations. For this reason we do not pursue the obvious Bessel function solution, which is a special case valid only for flat velocity profiles. Instead we favor a polynomial series expansion. The model plume function will be roughly Gaussian in the radial direction and roughly exponential in the axial direction.

Equation 12 is generally not separable. In fact, we anticipate strong coupling of the form r^2/z in our solution. We shall therefore insert an assumed asymptotic form into eq 12 and attempt to extract at least an approximate expansion in powers of r and z. Considering scaling arguments, we shall use a trial solution of the form

$$\gamma \sim -c_1\frac{k^{\mathrm{I}}z}{v_0} - c_{\mathrm{a}}s_2\frac{r^2v_0}{2Dz} + c_n\ln(z) \tag{17}$$

The first two terms in this series constitute a radial Gaussian, broadening and shrinking exponentially with increasing axial distance. The final term is nearly constant except for very small z. We use a coefficient naming convention in all of our expansions that has coefficients for terms of order m in z labeled c_m, coefficients of order n in r labeled s_n, and cross terms c_ms_n. Negative powers are labeled with letters starting with a. The term $c_n\ln(z)$ is motivated by the need to balance purely radial derivatives of the r^2 term, which will tend to leave terms of order $1/z$.

Inserting eq 17 into eq 12 with axial diffusion removed, we generate a polynomial

$$-k^{\mathrm{I}} + c_1k^{\mathrm{I}} + \frac{r^2\left(\frac{-(c_{\mathrm{a}}s_2{v_0}^2)}{2D} + \frac{c_{\mathrm{a}}{s_2}^2{v_0}^2}{D}\right)}{z^2} + \frac{-2c_{\mathrm{a}}s_2v_0 - c_nv_0}{z} = 0 \tag{18}$$

As this relationship must hold for all r and z, each coefficient must vanish. In this case an exact solution is easily obtained:

$$\{c_{\mathrm{a}}s_2 \rightarrow {}^1/_2,\ c_n \rightarrow -1,\ c_1 \rightarrow 1\} \tag{19}$$

which yields

$$\gamma_{\mathrm{flat}}(r,z) = -\frac{k^{\mathrm{I}}z}{v_0} - \frac{r^2v_0}{4Dz} - \ln(z) \tag{20}$$

Under these conditions dependence on XS appears in only the effective reaction rate constant term, and $k_{\mathrm{e}} = k$ exactly. It must be noted that this exact solution is only valid for wall-less flow, as it has a boundary condition of zero concentration at infinite radius; however, this condition is far more liberating than restricting, as it again emphasizes that the high-pressure flow technique is by design wall-less.

Laminar Flow. If one extreme flow condition is an essentially flat velocity profile, the other extreme is fully developed laminar flow, where the core velocity profile is highly curved. Under these conditions we expect the influence of radial diffusion on the effective rate constant to be at a maximum. Therefore, an approximate solution to the plume function for laminar flow that captures the influence of radial diffusion will define the upper limit of this effect. Our approach will mirror the approach we used to solve the plume function for a flat velocity profile, but we will require many more terms to adequately describe the various couplings. Fortunately, the potent derivative with respect to XS concentration will eliminate most of these terms.

For fully developed laminar flow, the diffusion constant, D, is independent of radius, and

$$v(r) = \left(1 - \frac{r^2}{{r_{\mathrm{w}}}^2}\right)v_0 \tag{21}$$

As with the flat velocity profile, we shall assume a trial solution as follows:

$$\gamma \sim -c_1\frac{k^{\mathrm{I}}z}{v_0} + c_2\frac{z^2}{2{v_0}^2} + c_n\ln(z) - c_{\mathrm{a}}s_2\frac{r^2v_0}{2Dz} + c_{\mathrm{a}}s_4\frac{r^4v_0}{D{r_{\mathrm{w}}}^2z} + c_{\mathrm{b}}s_4\frac{r^4{v_0}^2}{4D^2z^2} + s_2\frac{r^2}{2{r_{\mathrm{w}}}^2} + s_4\frac{r^4}{4{r_{\mathrm{w}}}^4} + c_1s_2\frac{r^2z}{{r_{\mathrm{w}}}^2v_0} \tag{22}$$

After inserting eq 22 into eq 12 and eliminating terms to first order in z and r^2 in the resulting polynomial, we find the following values for the coefficients to eq 22:

$$\left\{c_1 \rightarrow 1 - \frac{2D}{3k^{\mathrm{I}}{r_{\mathrm{w}}}^2},\ c_2 \rightarrow \frac{20D^2}{9{r_{\mathrm{w}}}^4} - \frac{4Dk^{\mathrm{I}}}{3{r_{\mathrm{w}}}^2},\ c_n \rightarrow -1,\ c_{\mathrm{a}}s_2 \rightarrow \frac{1}{2},\ c_{\mathrm{a}}s_4 \rightarrow \frac{1}{12},\ c_{\mathrm{b}}s_4 \rightarrow 0,\ s_2 \rightarrow \frac{1}{3},\ s_4 \rightarrow \frac{2}{9},\ c_1s_2 \rightarrow \frac{-k^{\mathrm{I}}}{3} + \frac{5D}{9{r_{\mathrm{w}}}^2}\right\} \tag{23}$$

The approximate plume function is

$$\gamma(r,z) \sim -\left(\frac{k^{\mathrm{I}}}{v_0} - \frac{2D}{3{r_{\mathrm{w}}}^2v_0}\right)z - \left(\frac{2Dk^{\mathrm{I}}}{3{r_{\mathrm{w}}}^2{v_0}^2} - \frac{10D^2}{9{r_{\mathrm{w}}}^4{v_0}^2}\right)z^2 - \ln(z) - \frac{v_0r^2}{4Dz} + \frac{v_0r^4}{12D{r_{\mathrm{w}}}^2z} + \frac{r^2}{6{r_{\mathrm{w}}}^2} + \frac{r^4}{18{r_{\mathrm{w}}}^4} + \frac{(5D - 3k^{\mathrm{I}}{r_{\mathrm{w}}}^2)}{9{r_{\mathrm{w}}}^4v_0}r^2z \tag{24}$$

Note that 3 of the 11 terms depend on k^{I}, so the derivative with respect to [XS] will greatly simplify the problem.

To test this model of plume development, we show in Figure 3 the spreading of an OH radical plume in laminar conditions (7 Torr, 12 m s^{-1} velocity). Data from each axis are fit to a Gaussian. The widths of these Gaussians are shown in Figure 3b, along with the evolution predicted by coefficient $c_{\mathrm{a}}s_2$ in the above model for a radical injector located 50 cm upstream of the first axis and a radical diffusion constant of 25 cm^2 s^{-1}. The dashed line is the same prediction with the injector location moved 10 cm closer to the first axis and the radical diffusion constant reduced by 20%. The functional form predicted by eq 24 is clearly consistent with the data, and while corrections to our assumed values are required to get a good fit to the data, neither the effective injector location nor the radical diffusion constant is known to high accuracy. Because the effective injection position may be different from the injector location due to extra mixing caused by either the injector or the presence of a high velocity jet, the injection position in particular is quite uncertain.

The good performance of eq 24 is very encouraging because most of the terms in the equation do not depend on [XS]. We do not need to be able to model the behavior of the plume itself to extract a rate constant; we only need to be able to model its dependence on [XS]. The fact that we can reasonably model the plume is a bonus.

We can now find the radial diffusion correction to the reaction rate constant. Inserting our plume function into eq 13, we find that most of the terms are eliminated, leaving only

$$k_{\mathrm{e}}^{\mathrm{I}} \simeq \left(1 + \frac{4Dz}{3{r_{\mathrm{w}}}^2v_0} + \frac{r^2}{3{r_{\mathrm{w}}}^2}\right)k^{\mathrm{I}} \simeq \left(1 + \frac{4Dz}{3{r_{\mathrm{w}}}^2v_0}\right)k^{\mathrm{I}} \tag{25}$$

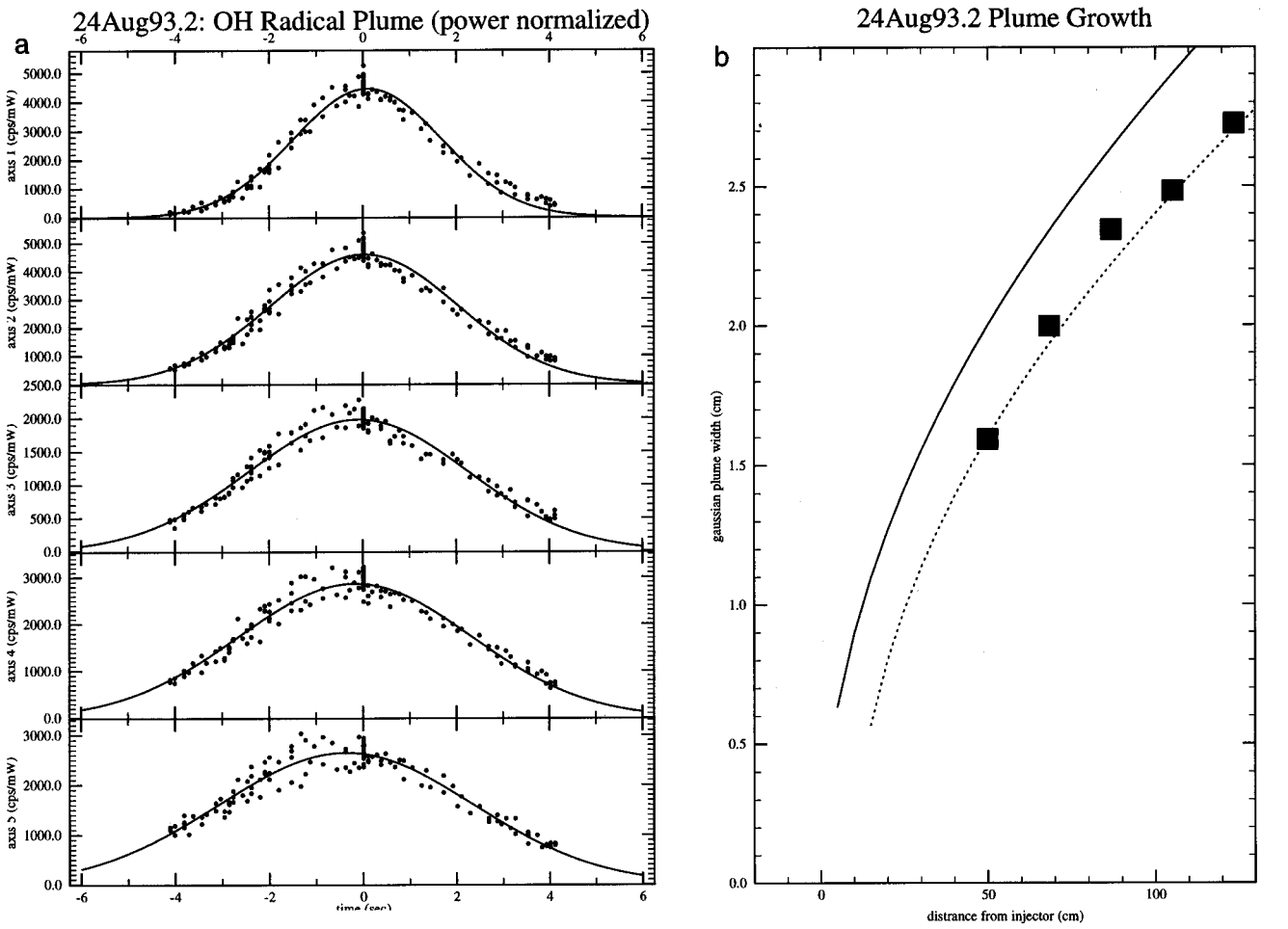

Figure 3. Radical plume growth in laminar conditions: (a) Gaussian plumes at each axis; (b) plume width as a function of distance from radical injector, data from (a) and a laminar model with two combinations of injector position and radical diffusion constant (the solid line is nominal values; the dashed line is adjusted slightly to fit the data).

We may safely drop the r^2 term when we image a small pixel along the spine of the radical plume. Note that this more rigorous expression is identical to the velocity correction based on scaling arguments shown in eq 16, save for a multiplicative factor of 4/3.

This correction depends on axial position and should thus be applied to the observed excess dependence ($\partial \ln C_0/\partial[\mathrm{XS}]$) before the axial derivative is taken. However, we can assess its magnitude by finding its value at the middle axis, located 88 cm from the injection point. For the example system, the radial diffusion term under laminar conditions is

$$\epsilon_{\mathrm{radical}} \approx \frac{4Dz}{3r_w^{\,2}v_0} = \frac{0.6}{p} \tag{26}$$

where pressure (p) is in Torr. Note that, since the diffusion constant for the radical in the bath gas will be proportional to the viscosity of the gas, under laminar conditions

$$\epsilon_{\mathrm{radical}} \approx \frac{4}{3}(\chi \mathrm{Re} r_w)^{-1} \tag{27}$$

where Re is the Reynolds number and χ is the proportionality constant between the carrier gas viscosity and the diffusion constant of the radical. The radial diffusion correction can therefore be kept tolerably small (<0.2) at low pressures by increasing the core velocity.

Turbulent Flow. The laminar solution was relatively simple in large part because of the exact (and simple) solution for the laminar velocity profile. Turbulent velocity profiles, even considering only the mean profiles, are far more complicated, generally not yielding to exact or even simple approximate solutions. They are characterized by very large shear near walls and relatively small shear near the core of a tube. There can be no "flat" velocity profile for well-developed turbulence, as curvature in the velocity profile is the sole means of producing a shear force to balance the ubiquitous (and radially constant) pressure gradient force. The velocity profile must therefore be at least quadratic, though the radius of curvature may be much larger than the actual radius of the flow tube.

The simplest picture of the core velocity profile in fully developed turbulence is thus that one finds a laminar (parabolic) profile with an effective tube radius (r_e) greater than the actual tube radius. Using an eddy diffusivity model of turbulence with a eddy diffusion constant, D_e, which is a function of bulk velocity and a weak function of radius (far from the tube wall), one can show that a fourth-order polynomial will adequately describe a turbulent velocity profile between the core of a tube and roughly half the distance to the wall. A derivation of this result may be obtained from the authors. Data for 66 Torr of nitrogen in the 6.15 cm radius HPF system (Re = 11 000) are shown in Figure 4. The curve in the figure is a parabolic fit, showing that at this Reynolds number, the polynomial expansion of the velocity profile converges even more quickly in the core of a flow than our model predicts. This establishes that the eddy viscosity in the core of the HPF system is effectively constant, and the above effective radius argument is valid. We can define the effective radius, r_e, based on our velocity profile model:

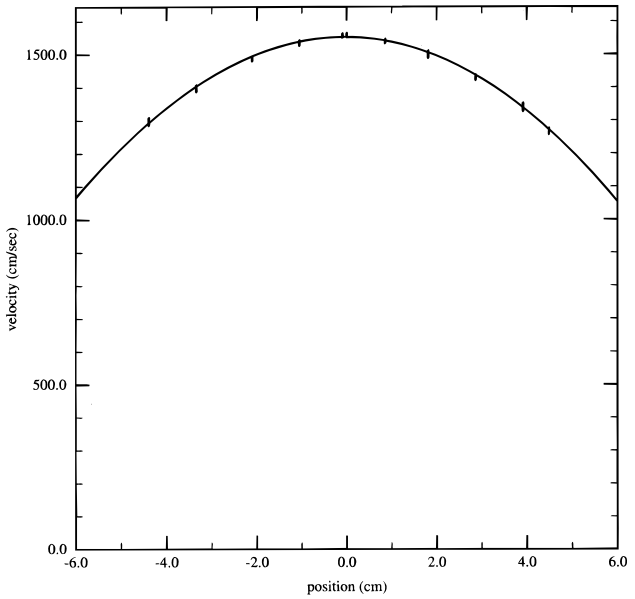

Figure 4. Turbulent velocity profile, Re = 11 000. The curve through the data is a second-order fit, showing that truncation of the turbulent velocity profile at second order is valid for the core velocity profile under these conditions.

$$r_e = \sqrt{\frac{4D_e v_0}{H}} \tag{28}$$

where H is the pressure head. The effective radius for the profile in Figure 4 is roughly 12 cm.

Turbulent Radial Diffusion. To develop a radial diffusion correction for turbulent flow, we assume that the preceeding treatment of the turbulent velocity profile is qualitatively correct. In particular, we assume a core velocity profile of the form

$$V(r) = V_0 - a_2 r^2 - a_3 r^3 - a_4 r^4 \tag{29}$$

with an eddy diffusion constant

$$D(r) = \epsilon V_0 (r_w - r) + D_w \tag{30}$$

The values of the parameters in both equations are left to a fit of velocity data.

The solution proceeds in parallel with the laminar solution, though the algebra is considerably more complicated. The result for the plume function is extensive and may be obtained from the authors on request. However, the expression for the effective rate constant remains simple, as the vast majority of the terms in the turbulent plume function do not depend on the first-order loss rate. Using eq 13 for the effective rate constant, we find

$$\begin{aligned} k_e^I &= \left(1 + \frac{a_2 r^2}{3V_0} + \frac{4a_2 D_w z}{3{V_0}^2} + \frac{4a_2 \epsilon r_w z}{3V_0}\right) k^I \\ &\simeq \left(1 + \frac{4a_2 z}{3{V_0}^2}(\epsilon r_w V_0 + D_w)\right) k^I \\ &= \left(1 + \frac{4a_2 z}{3{V_0}^2} D_0\right) k^I \end{aligned} \tag{31}$$

which is identical to the laminar correction, eq 25, with $a_2 = V_0/{r_w}^2$ in the laminar case, and D_0 the core diffusion constant in this case.

We have now established both that the turbulent velocity correction for a fourth-order turbulent velocity profile is identical in form to that for laminar flow and that, if anything, actual turbulent velocity profiles are even more parabolic in the core than our model predicts. We can thus very safely assume that the eddy-diffusion coefficient in the core of the flow is effectively constant and that the core velocity profile is parabolic. This provides a potent handle for our problem, because radial stress in the tube must be constant, as the pressure may not be a function of radius. This permits us to apply measurements of the pressure head at the pipe wall, where the eddy diffusion coefficient is surely changing rapidly with radius, to the stress in the core of the pipe, where the eddy diffusion coefficient is effectively constant. If we further assume that the eddy diffusion coefficients for momentum and scalars are identical, we can greatly simplify the problem.

The stress balance for incompressible Poiseuille flow produces a laminar velocity profile

$$v(r) = \frac{1}{4\mu}({r_e}^2 - r^2)\frac{\partial p}{\partial z} \tag{32}$$

Relating the viscosity to the diffusion coefficient with $\mu = D\rho$ and using the ideal gas law, we get

$$\frac{\partial^2 v}{\partial r^2} = \frac{RT}{2DM_w}\frac{\partial \ln p}{\partial z}$$

so

$$2a_2 = \frac{RT\eta}{2DM_w}$$

$$D = \frac{RT\eta}{4a_2 M_w} \tag{33}$$

where η is the fractional pressure head and a_2 is the second-order term in the velocity polynomial. Combining eqs 31 and 33 yields

$$k_e^I = \left(1 + \frac{RT\eta z}{3M_w {V_0}^2}\right) k^I \tag{34}$$

This expression is very similar in form to eq 25, and it is based entirely on quantities that are either well-known or easily measured in our flow tube.

Radial Diffusion Corrections to the Reaction Rate Constant. We are now able to offer a revised expression for the experimental reaction rate constant in a high-pressure flow system (eq 7). Including the effects of radial diffusion, we find

$$\begin{aligned} k &= -V_0 \frac{\sigma l}{\zeta}\frac{\partial}{\partial z}\left(\epsilon_D \frac{\partial}{\partial \tau}\ln\frac{S(z)}{S(i)}\right) \\ \epsilon_D &= \left(1 + \frac{2Dz}{3{r_w}^2 V_0}\right)^{-1}, \quad \text{(laminar flow)} \\ &= \left(1 + \frac{RT\eta z}{6M_w {V_0}^2}\right)^{-1}, \quad \text{(turbulent flow)} \end{aligned} \tag{35}$$

where V_0 is the core velocity, σ is the appropriate absorption cross section, l is the absorption path length, ζ is the ratio of reagent to tracer, z is axial position, τ is observed (reagent or tracer) optical depth, S is radical signal, D is radical diffusion constant, r_w is tube radius, η is fractional pressure head, and M_w is the molecular weight of the carrier gas. The correction

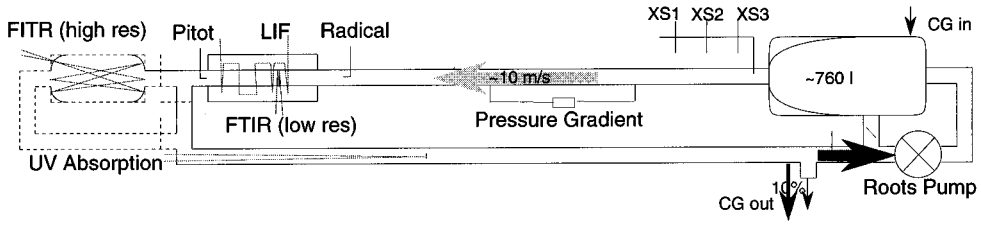

Figure 5. High-pressure flow system. The system description begins in the upper right corner of the figure and proceeds counter clockwise. Carrier gas (usually N_2) flows into the ~760 L settling chamber through calibrated mass flow controllers. Reagents are injected automatically from one of several manifolds located either at the settling chamber of just downstream of the settling chamber. The flow passes through a 10 m entrance length of 12 cm tubing, along which the down-tube pressure gradient is measured. Radicals are injected into the core of the flow 50 cm upstream of a laser induced fluorescence detection zone consisting of five detection axes spearated by 18.4 cm. Fluorescence is detected with photomultipliers attached to each axis with a liquid light guide, which may be scanned as a group across the radius of the tube, developing a two-dimensional image of the radical plume. Between axes 1 and 2 is a multipass IR White cell (12 cm base path, up to 48 pass), coupled to a medium resolution (0.25 cm^{-1}) FTIR spectrometer (Mattson RS1). A pitot static tube at the end of the detection zone measures velocity as a function of radius. Flow after the detection zone may be either shunted to the return path or allowed to pass through a multipass Harriot cell (1 m base path, up to 20 pass) coupled to a high-resolution (0.002 cm^{-1}) FT spectrometer (Bruker HFS 120). The first 3.5 m of the return axis comprises a 7 m (2 pass) UV absorption axis used to measure reagent concentrations. Carrier gas is removed from the system immediately upstream of a gate valve. Any fraction (0−100%) may be removed. Remaining carrier gas is forced by a Roots blower back through the settling chamber, where a fraction may be shunted back to the blower, thus regulating the flow in the main tube.

factor is applied before the axial gradient is taken, as it has the effect of removing a small axial curvature from the data. This correction removes the last theoretical obstacle to developing absolute discharge flow rate constant measurements with extremely high accuracy.

As we have shown, the measurements may be conducted over an extremely wide dynamic range of pressures (3 orders of magnitude). In addition, while the theory described here depends on minimal interaction with the wall, it also introduces a factor with a straightforward interpretation as the amount of wall contact. When the radial diffusion correction cuts the derived rate constant in half, diffusion to the wall is significant; conversely, when the radial diffusion correction is 10% or less, wall interactions may be safely neglected. In our system, this latter condition holds for all but the very lowest pressures ($p <$ 5 Torr). The absence of wall interactions in turn clears the final hurdle to making discharge flow measurements at very low temperatures ($T <$ 200 K), such as are found in the upper troposphere and lower stratosphere of the earth's atmosphere. It is at these temperatures and pressures that weakly bound intermediates in radical molecule reactions result in the unusual pressure and temperature dependencies discussed in the introduction to this paper.

High Pressure Flow System

Experimental Description. The HPF apparatus used in this work is a modification of the original system described in A90. A schematic of the system is shown in Figure 5. Aspects of the experiment unchanged from A90 will be described only briefly. The most noteworthy modification is a complete redesign of the OH radical injector, discussed below. Second to this is a modification of the system layout to allow operation of the system with or without carrier gas recirculation. Third, a medium-resolution FTS (Mattson RS1, 0.25 cm^{-1}) and a high-resolution FTS (Bruker 120HR, 0.002 cm^{-1}) have also been added to the system; these instruments, whose primary purpose is spectroscopic analysis, are critical to the objectives of research on intermediates but will be discussed in this paper only to the extent that they improve our ability to measure excess reagent concentrations.

Flow Regulation and Measurement. A well-developed carrier flow (N_2) is established by pumping the diluent with a roots blower first through a large (~700 L) settling chamber then down a long (10 m) section of 12.36 cm i.d. pipe. The flow passes through the main kinetics test section, where radicals are introduced and measured, and then returns to the Roots pump along a second pipe. The carrier gas is continuously refreshed by pumping off a fixed fraction at the end of the return pipe and replacing this with fresh carrier gas in the settling chamber. This fraction can range from 0 to 100% of the full flow; a typical value is 10%. Pressure is controlled primarily by controlling the fresh carrier mass flow and secondarily by adjusting the exhaust volume flow rate. The total system volume is 890 ± 15 L. Gas residence times in the system are typically 1−2 min, though times as low as 30 s are used in some kinetics experiments. The velocity of the main flow is controlled by adjusting a throttle valve in a shunt pipe connecting the settling chamber to the head of the Roots pump. Kinetics are generally performed with core velocities ranging from 5 to 15 m s^{-1}.

Flow characteristics are evaluated by monitoring both the down-tube pressure gradient and the pressure differential in a pitot-static tube. The pressure gradient along the middle 10 ft section of this pipe is measured with a differential capacitance manometer (MKS 220, 1 Torr). In fully developed, laminar, incompressible flow (Poiseuille flow) this pressure gradient is related to the core velocity (e.g., Batchelor [1967]).

$$V_0 = \frac{r_w^2}{4\mu}\frac{\Delta p_g}{\Delta z} \tag{36}$$

where r_w is the radius of the tube, μ is the viscosity and Δp_g is the pressure differential measured over a distance Δz. A pitot tube just downstream of the fifth LIF axis is used to measure the flow velocity; differential pressures in the pitot tube are measured with a second differential manometer (MKS 398, 1 Torr). The pitot tube reading is directly related to velocity by

$$V = \sqrt{\frac{2RT\delta p_p}{Mp}} \tag{37}$$

where Δp_p is the pitot-static differential pressure, M is the molar weight of the carrier gas, and p is the system pressure. The original, long, pitot tube entering from the end of the flow system (described in A90) has been replaced with a right angle pitot tube fixed behind the fifth axis. This change allowed the addition of a multipass absorption cell to the end of the flow system. The two tubes yield identical results in simultaneous tests. In laminar conditions the pitot tube and pressure gradient measurements typically agree to within 5%.

A third measure of the well-developed laminar core velocity may be obtained when the system is operated in a nonrecirculating mode. Carrier gas flow into the HPF system is regulated with calibrated mass flow controllers; in the absence of recirculation, this direct measure of the bulk flow can be trivially converted into the core velocity. This measure also typically agrees with the others to within 5%. Because the sources of systematic error in eqs 36 and 37 and the single pass bulk-flow method are distinct from one another, we regard this 5% agreement as an indication of the accuracy of our velocity measurements under laminar conditions. This pitot tube measurement is currently the sole measure of turbulent velocities. We feel that the estimated 5% error is valid under these conditions as well for the following reasons: the pitot-static signal is proportional to system pressure, turbulent conditions obtain at higher system pressures, and there is no *a priori* reason to suspect that the pitot tube accuracy declines in conditions of modest turbulence.

Radical Preparation. Radicals are prepared in a side arm and injected with a single narrow (3 mm) quartz injector directed into the flow in order to cause minimal flow disturbance. Radial diffusion widens the plume and mixes it sufficiently for our needs by the time it reaches the first radical detection axis. This change in injection strategy from the four radial pipet injectors of A90 substantially reduces the residence time of radicals (both hydroxyl and hydroxyl precursors) in the radical source and makes the source easier to control. It also produces the narrowest possible plume; as this work will show, this is a highly desirable characteristic. We currently employ two OH radical sources. Either dilute hydrogen or dilute fluorine in helium or argon carrier is dissociated by passing the mixture through a microwave induced plasma (MIP). The resulting atoms are titrated with an excess of NO_2 or H_2O to produce OH. OH concentrations are kept as low as possible to minimize the generation of secondary radicals, particularly O atoms, by OH self-reaction.

The total flow from the radical source is restricted to less than 1% of the bulk flow in the HPF system. This minimizes flow disturbance and also ensures that the excess reagent present in the bulk flow will completely diffuse into the evolving radical plume before the plume reaches the first radical detection axis. This "healing" of the excess reagent profile is vital to the success of the experiment. Fortunately, the return of the excess reagent to the core of the flow is nearly the inverse problem of the outward diffusion of the radicals, and we directly measure the latter. An analysis of eq 24 indicates that a 1% source flow to bulk flow ratio is safe; for example, if the original width of the plume shown in Figure 3 was 1% of the width of the tube (which is 1% of the bulk flow in laminar conditions), the excess reagent at the center of axis 1 would be roughly 3% below its mean value.

A second requirement on the radical source is that the radical concentration be kept sufficiently low to guard against interference by secondary reactions (Vaghjiani and Ravishankara [1991]). Many radical molecule reactions produce at least one highly reactive radical as a product. It is prudent to assume that this product radical will react with the primary radical on every collision ($k^{2nd} \sim 10^{-10}$ cm^3 molecules^{-1} s^{-1}). Furthermore, the rate of primary radical reaction with the primary reagent is fixed by the experimental design; in our case, the characteristic first-order loss rate of radical is $k^I = 10$ s^{-1}. Assuming that the reaction produces an amount of secondary radical equal to the initial radical concentration, we have the following simple expression for the safe limit of radical concentrations:

$$[R]_0 k^{2nd} \ll k^I$$

$$[R]_0 \ll 10^{11} \text{ molecules cm}^{-3} \tag{38}$$

This is a very severe requirement; good kinetics requires radical measurement with high signal to noise over at least two decades in concentration. Therefore, in order to be certain that secondary reactions contribute less than 1% toward the observed radical removal, the radical detection limit must be on the order of 10^7 molecules cm^{-3} or better. Where this requirement is not met, the secondary radical reactions must be carefully considered. If k^{2nd} is known to be slower than gas kinetic, the restriction relaxes; otherwise the secondary radical must be chemically scrubbed from the system before it has an opportunity to react with the primary radical.

Radical Measurement. Some 50 cm downstream of the radical source is the first of five OH LIF axes, each separated from the next by 18.4 cm. A 282 nm laser beam passes twice through the first, second, and fifth axes and once through the third and fourth. The LIF axes are otherwise unchanged from those described in A90; however, the LIF laser has been substantially modified. We now use a Nd:YLF laser (Spectra Physics TFR) to pump the etalon narrowed tunable dye laser (Chromatix) at 2500 Hz. Fluorescence at 309 nm from a small (<1 cm) radial pixel in the radical plume is detected in the manner described in A90. Because of the relatively low pulse repetition frequency, photon detection is limited to a single event per laser pulse by broadening event peaks in the amplifier/discriminator to a width greater than the (500 ns) counter gate width. Apparent count rates are then statistically corrected to their true values with the formula

$$S = -\nu \ln\left(1 - \frac{S'}{\nu}\right) \tag{39}$$

where ν is the laser pulse repetition frequency and S' is the observed count rate (Wennberg et al. [1994a]). We have added a stepper motor to the etalon armature, facilitating automatic scanning over OH LIF lines. In normal operation the laser is held on the center of an OH line and periodically moved roughly two line widths off line to monitor the nonresonant scattering background.

Reagent Measurement. A 7 m UV absorption cell on the return path remains identical to that described in A90. We follow the strategy described in A90 of mixing reagents with a nonreactive tracer (CF_2Cl_2) and then monitoring the UV absorption signal of this tracer as a surrogate for the reagent. For all of our work, UV absorption was measured on the 1849 Å Hg line, where absorption by the tracer almost always overwhelms that by the reagent. This measurement requires accurate knowledge of the F12 absorption cross section; we measure the cross section to be $(121 \pm 6) \times 10^{-20}$ cm^2, in excellent agreement with the value recommended in JPL [1994].

Reagent−tracer mixtures are carefully prepared on a gas manifold, with the reagent/tracer ratio determined by pressure measurements. FTIR validations have show better than 1% reproducibility in the mixture preparations. While this method relies on the assumption that the reagent/tracer ratio remains constant during a run (and thus that evacuation from the system is the dominant loss mechanism for each), this assumption has proven to be valid for a very large fraction of reagents. Assuming that the chemical sink term for the reagent is simply the flux of radicals out of the radical source, we can write a simple expression for the loss flux of a reagent in our system

$$\Phi_{XS} = \Phi_{OH} + [XS]\frac{V}{\tau} \tag{40}$$

where V is the system volume (~1000 L) and τ is the system flushing time scale (~100 s). The radical flux is roughly 10^{15} s^{-1}, as an upper limit; it is often a factor of 10 lower. The reagent concentration is fixed by our experiment; we are most sensitive to radical decay when the first-order decay rate is approximately 10 s^{-1}, so [XS] ~ 10/k. Thus, for mechanical pumping to dominate the radical loss term,

$$k \ll \frac{10}{\Phi_{OH}}\frac{V}{\tau}$$

$$\sim 10^{-10}\ \text{cm}^3\ \text{molecules}^{-1}\ \text{s}^{-1} \tag{41}$$

Under the conditions specified, our passive tracer measurement can be used as a substitute for the reagent measurement only for reactions with reaction rate constants less than roughly 10^{-11} cm^3 $molecules^{-1}$ s^{-1}. Above this value we must carefully assure the validity of the above assumption. The critical reaction rate constant can be increased by reducing the system pumping time scale and by reducing the radical flux. This is one of very many reasons for maintaining as high a radical sensitivity as possible.

The UV absorption method is being augmented by low-resolution FTIR measurements carried out in a radially oriented White cell (15 cm base path, Hanst) located between the first and second LIF axes. While the FTIR offers specificity and very high signal to noise, it suffers from uncertainty in the total path length in a cell with recessed mirrors as well as temperature- and pressure-dependent cross sections, which are often not well-known. Data analysis is also more complicated. The UV tracer measurement, with its ease of use, temperature-independent cross section, and well-known path length, thus retains considerable utility.

Temperature Measurement. The flow temperature is measured with thermistors in three locations: at the pitot tube just downstream of the fifth LIF axis, at the head of the UV absorption axis, and at the end of the UV absorption axis. Temperature measurements are accurate to within 1 K. The reaction temperature is assumed to be the temperature measured at the pitot tube. If the temperature measured in the UV absorption axis differs from the reaction temperature, the concentrations measured there are corrected for the density change between the two locations. For the room temperature rate constants discussed in this paper there are no significant temperature gradients in the system, so the density correction is extremely small.

System Operation. Reagent tracer bulbs are mounted on a manifold connected to the head of the main flow tube, just downstream of the settling chamber. This manifold can accommodate several reagent bulbs (currently four) and is fully computer controlled. Roughly 3 min into a typical 15 min kinetics run, the computer opens a valve connecting this manifold to the flow system, allowing a specified quantity of reagent from a selected bulb into the system. The reagent rapidly mixes in the HPF system and is subsequently removed by evacuation on a 1−2 min pumping time scale along with the carrier gas. During this interval, the reagent concentration in the system and the radical signal at each of the five LIF axes are all monitored; this constitutes the two derivatives of radical signal with respect to axis and reagent concentration necessary to determine a reaction rate constant.

Data Analysis. The course of a run and the subsequent data analysis are illustrated in Figure 6 for a determination of the OH + ethane reaction rate constant at 299 K and 36 Torr nitrogen in turbulent flow, using the rapid bimolecular reaction

$$H + NO_2 \rightarrow OH + NO$$

as an OH source.

Figure 6a shows the UV absorption signal of the passive tracer at 1849 Å. This data is fit to an exponential removal model that includes terms for the UV baseline, a linear baseline drift, the injection time, the duration of the injection pulse, the injection size, and the system evacuation time scale. The residuals of this fit are also shown in Figure 6a along with 95% confidence lines and a smoothed plot of the residuals, showing that the model sufficiently describes the data. The results of this model are used to calculate the excess reagent concentration as a function of run time.

Figure 6b shows the OH signal at each of the five LIF axes as a function of run time. For the first axis the power normalized signal is shown; for each subsequent axis, the signal normalized by the axis 1 signal is shown.

Figure 6c results from the combination of the first two data streams; it shows the (axis 1) normalized radical signal for axes 2−5 as a function of modeled excess concentration. The figure includes both raw (1 Hz) and binned data for clarity. To avoid overwhelming the analysis with data for very low excess reagent concentrations, the data set is arbitrarily truncated, usually at an excess reagent concentration a factor of 50 below the maximum concentration. Each axis signal is also normalized by the average signal at that axis prior to the injection. The plots for each axis are offset to prevent undue overlap. Under pseudo-first-order conditions each log intercept should thus be the log of the offset multiplier, which is indicated by a colored tick.

Because the excess reagent concentration decreases continuously to zero, the pseudo-first-order assumption requires closer than normal examination. The requirement of pseudo-first-order kinetics is not actually that the excess reagent concentration be much greater than the radical concentration, but rather that the excess reagent concentration not change significantly in the reaction zone. At low reagent concentration there is often little reaction, especially if the radical concentration is also kept low, so in many cases the reagent concentration will remain constant even if it is lower than the radical concentration. For pseudo-first-order conditions to hold, either [XS] must be much greater than [OH] or the lifetime of XS (k[OH]) must be much longer than the transit time from the radical injector to the final detection axis. Thus, for sufficiently low first-order loss rates of XS (i.e., sufficiently low [OH]), pseudo-first-order conditions will hold for all [XS].

Note that the raw axis 1 data, were they plotted in Figure 6c, would lie roughly on top of the axis 3/axis 1 data. Any qualitative assessment of linearity must account for this. The linear range of the axis 5/axis 1 data is roughly a factor of 30 in radical signal, after which the signal curves upward slightly; over this same range, the raw axis 1 signal declines by roughly a factor of 3. The data shown therefore depict an experiment that marginally passes the canonical requirement that decays display 2 decades of log-linear behavior. This form of presentation accentuates the effects of secondary chemistry, because it emphasizes large non-dimensional reaction times. This in turn helps the experimenter identify and eliminate secondary chemistry problems.

Figure 6d is derived from the previous plot. It shows the slopes from that plot as a function of axis number. The nominal zero slope for axis 1 is also included. These data should be linear, and their slope, once scaled by the measured velocity, may be interpreted as the reaction rate constant.

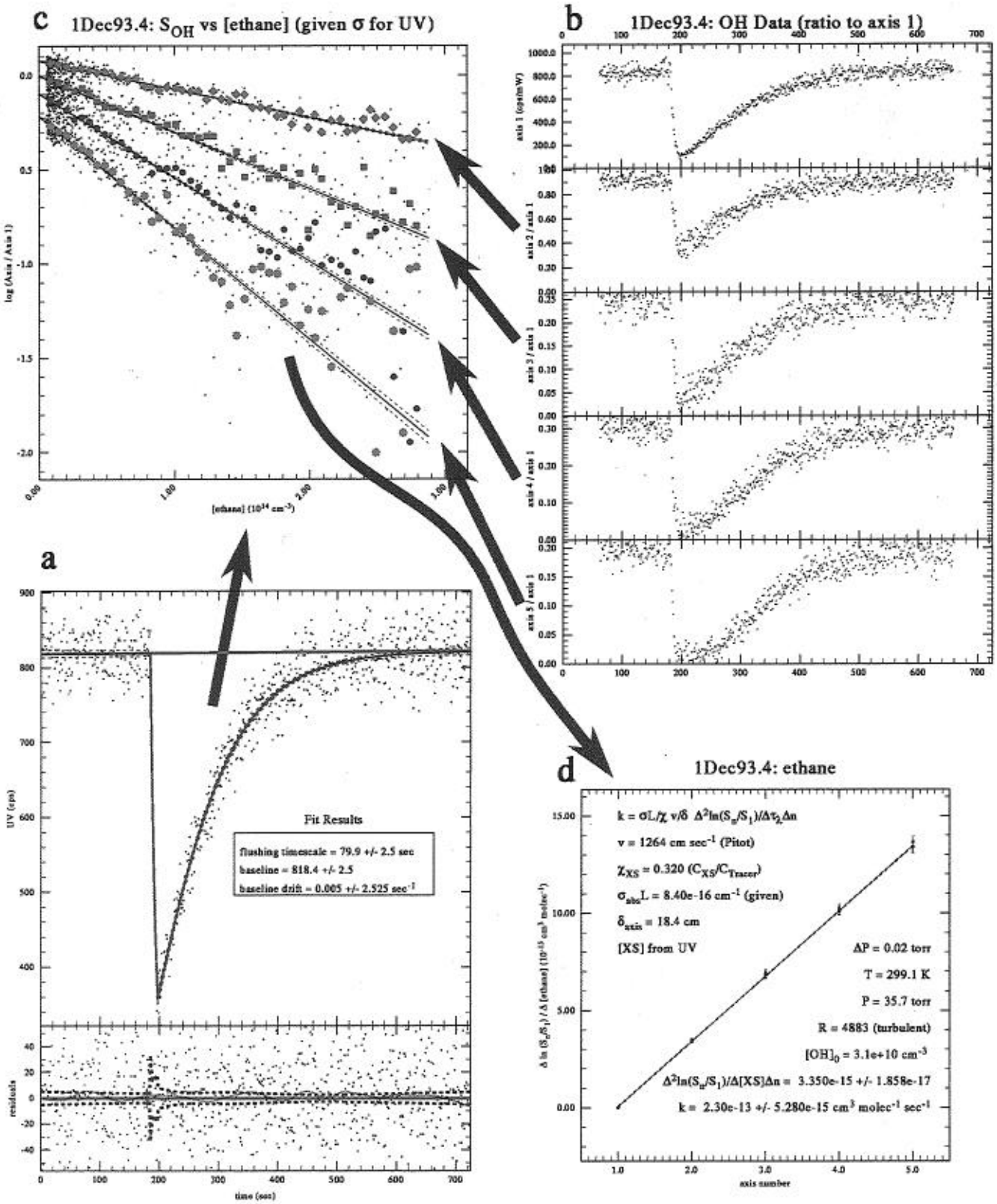

Figure 6. Stages in HPF data reduction. Excess reagent [XS] is measured with long-path absorption (a). The exponential diminution of the absorption signal is due to carrier gas turnover in the system. The radical LIF signal for each detection axis responds to the changing [XS] (b). These XS and radical time traces are combined to give $\ln(S_n/S_1)$ for LIF axes 2−5 (c). The slopes of these lines in turn become data for the final plot (d), which, combined with the measured core flow velocity, yields the rate constant.

Results

Rate Constant Measurements. In order to examine the validity of our data analysis method, we have measured two bimolecular reactions under a very wide range of experimental conditions.

$$\text{OH} + \text{ethane} \rightarrow \text{products} \quad \text{(R1)}$$

$$\text{OH} + \text{cyclohexane} \rightarrow \text{products} \quad \text{(R2)}$$

The results of some 50 determinations of the OH + ethane rate constant are shown in Figure 7. Runs below 20 Torr are in laminar flow conditions. For these cases the down-tube

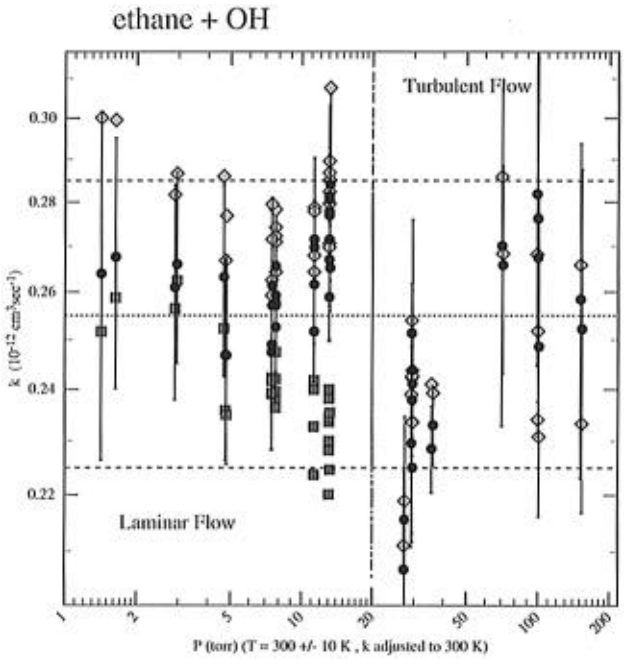

Figure 7. Rate constant measurements for OH + ethane. Raw data (corrected to 300 K) are shown as gray diamonds. Diffusion-corrected data are shown as black circles, with error bars. Measurements below 20 Torr are in laminar flow. Those above 20 Torr are in turbulent flow. Laminar velocity determinations are based on the pressure head measured in the HPF system. Rates based on pitot-static velocity measurements are shown as gray squares. Our best estimate rate constant ($(2.55 \pm 0.3) \times 10^{-13}$ cm^3 molecules^{-1} s^{-1}) is shown as a horizontal dashed line, along with 95% confidence limits.

pressure gradient has been used to infer the peak velocity, as the pitot tube signal becomes very noisy at low pressures. For turbulent cases, the pitot tube has been used to directly measure the core velocity. All data have been corrected for radical diffusion effects as discussed in this paper. The data are corrected to 300 K, using an activation energy of 1060 K (Atkinson [1991]). The actual range in temperatures in the data set is from 295 to 305 K, with the higher pressure data systematically warmer because of frictional heating in the system. The error bars combine the estimated precision of each run (which is a byproduct of the analysis described above) and an additional estimated error based on the quality of the run. The run quality is assessed by examining the plots shown in Figure 6 for linearity, appropriate intercepts, and absence of baseline drifts. Aside from the occasional run rejected as being clearly flawed, the runs are grouped in three categories, with an estimated additional experimental error of 2.5, 7.5, and 12.5% added in quadrature to the experimental precision, depending on the category. These values, while obviously somewhat arbitrary, are based on the assessment of thousands of runs over several years.

The radial diffusion correction clearly removes much of the pressure-dependent variation in the raw data. This is most evident at low pressures, as expected. The OH + ethane reaction is purely bimolecular, so we may safely conclude that all evident sensitivity to pressure in the observations is due to uncorrected systematic errors. Because most of the remaining deviation from pressure independence lies near the transition from laminar to turbulent flow, it is likely that there are errors caused by ill-conditioned flow; however, we have yet to identify the cause of these effects.

The OH + ethane data shown are but a small subset of our total data set for this reaction. They were selected for this presentation because they are all taken in conjunction with

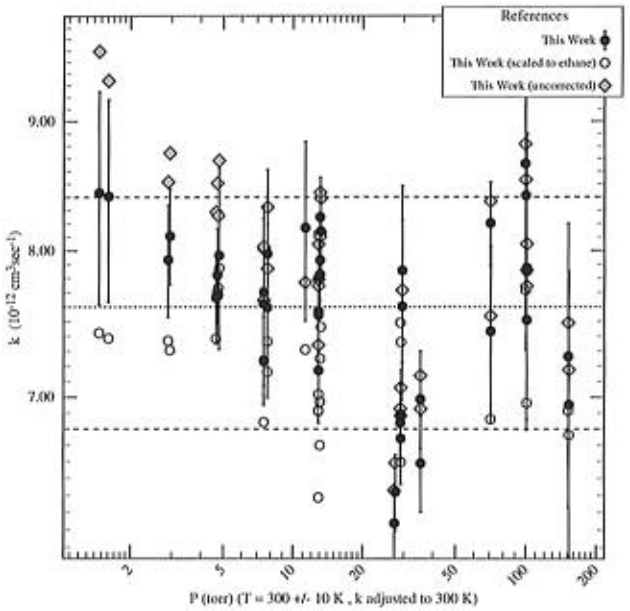

Figure 8. Rate constant measurements for OH + cyclohexane. Raw data (corrected to 300 K) are shown as gray diamonds. Diffusion-corrected data are shown as black circles, with error bars. Data normalized with corresponding ethane + OH rates are shown as open circles. Our best estimate rate constant ($(7.6 \pm 0.8) \times 10^{-12}$ cm^3 molecules^{-1} s^{-1}) is shown as a horizontal dashed line, along with 95% confidence limits.

measurements of the OH + cyclohexane reaction. Those measurements are shown in Figure 8. The figure shows raw measurements, measurements corrected for radial diffusion, and the ratio of each uncorrected measurement to the corresponding OH + ethane measurement. The latter have been scaled by an assumed OH + ethane rate of 2.45×10^{-13} cm^3 molecules^{-1} s^{-1} at 298 K (JPL [1994]). As with the OH + ethane reaction, the radial diffusion correction removes nearly all of the dependence on pressure, leaving only a small set of data taken in low Reynolds number turbulent flow systematically lower than the other data. More of the systematic variation with pressure is removed by normalizing the OH + cyclohexane measurements to corresponding OH + ethane measurements. Even the low data just mentioned is brought into agreement with the rest of this data. This is consistent with eq 8, which predicts not only that most systematic effects of fluid dynamics will be removed by the normalization but also that the resulting data will be more precise than even the diffusion-corrected raw data.

Discussion. Our fully analyzed results are shown in Figures 9 and 10, along with many other published measurements of these two rate constants at room temperature and a wide range of pressures. Other studies are plotted as a single point at their mean pressure; it is possible to identify the general class of experiment (discharge flow, flash photolysis) by the pressure. In each case the agreement with the literature is excellent. However, in order to assess our overall confidence in these measurements, we must address potential causes of error other than radial diffusion, especially secondary chemical reactions.

In most cases the OH concentration is below 10^{11} molecules cm^{-3}. However, this is well over the limit (eq 38) where secondary reactions may contribute to the observed OH decay. We do not observe a significant increase in the rate constant with increasing OH concentration, which would be a sign of such a problem. Through leaks and impurities in our carrier gas, the oxygen concentration in the HPF system currently never falls below roughly 10^{15} molecules cm^{-3}. At this level, alkyl radicals produced by the initial abstraction will react very rapidly

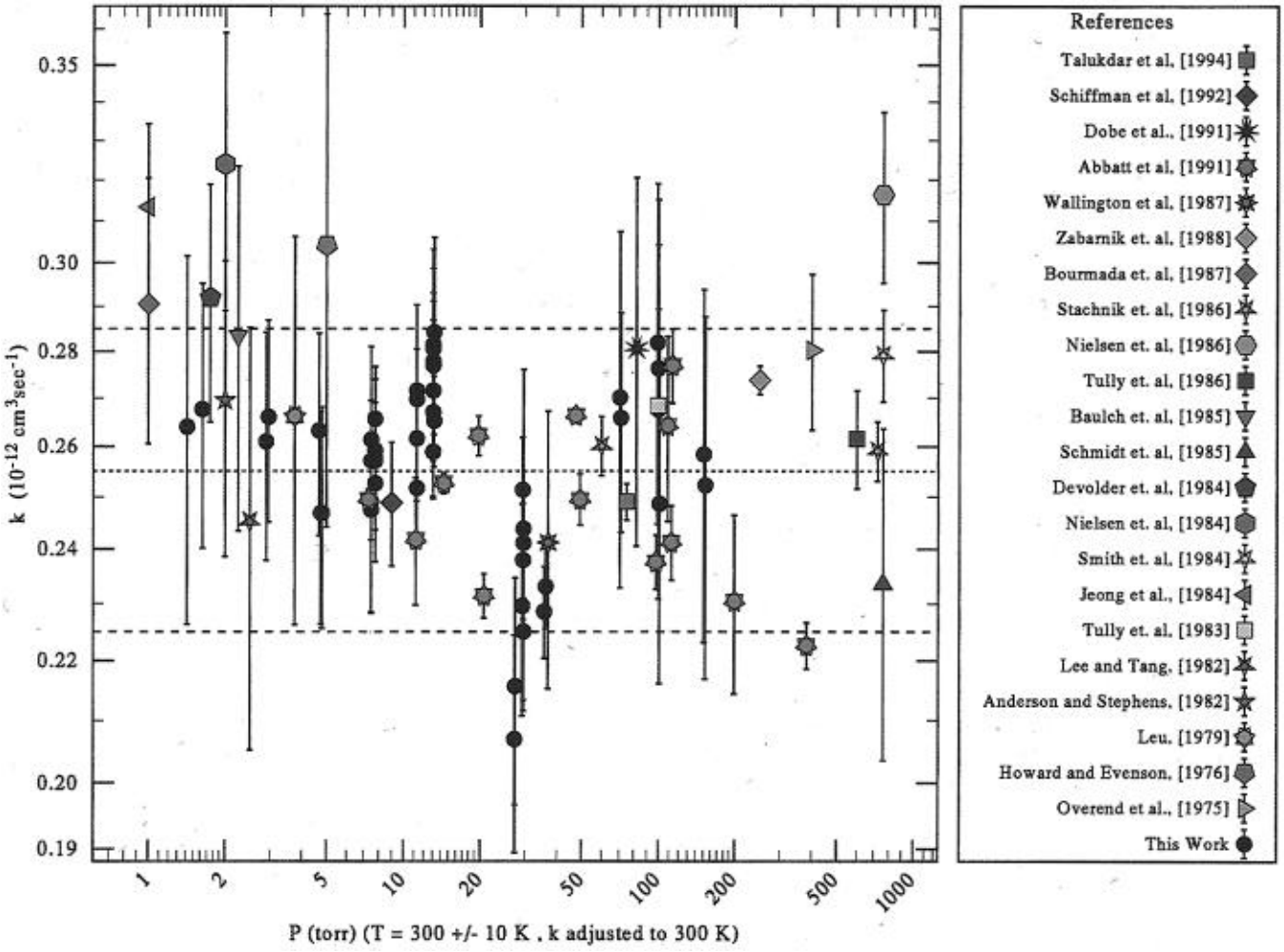

Figure 9. Diffusion-corrected rate constants for OH + ethane. Our best estimate rate constant ($(2.55 \pm 0.3) \times 10^{-13}$ cm^3 molecules^{-1} s^{-1}) is shown as a horizontal dashed line, along with 95% confidence limits. Data from other published studies are shown with the symbols indicated in the legend. All values are corrected to 300 K.

($\sim 10^{-4}$ s) to form organoperoxy radicals (RO_2). The RO_2 may in turn react with NO_x emitted by the OH source ($H + NO_2 \rightarrow OH + NO$) to form organic nitrates, as the source is in general operated in large excess of NO_2. The RO_2, and certainly the organic nitrates, will be far more stable than the alkyl radicals with respect to OH reaction. Therefore, while secondary OH removal remains a potential problem in these reactions, we do not believe that it significantly contributes to the observed rate.

A second potential problem is OH generation in secondary reactions. The following multistep process (well-known in the atmosphere, Logan et al. [1981]) can occur very rapidly in our flow system:

$$RH + OH \rightarrow R + H_2O \quad \text{(R3)}$$

$$R + O_2 \rightarrow RO_2 \quad \text{(R4)}$$

$$RO_2 + NO \rightarrow RO + NO_2 \quad \text{(R5)}$$

$$RO + O_2 \rightarrow R{=}O + HO_2 \quad \text{(R6)}$$

$$HO_2 + NO \rightarrow OH + NO_2 \quad \text{(R7)}$$

Assuming roughly 1 ppm oxygen present as a contaminant in our carrier gas (augmented by leakage into the system), with the residual NO_x from the OH radical source, the rate-limiting step in this sequence is reaction R6, the hydrogen abstraction from an alkoxy radical, producing a carbonyl and the hydroperoxy radical. Typical rate constants for R6 are $k_6 \sim 10^{-15}$ cm^3 molecules^{-1} s^{-1}. With oxygen levels of 3×10^{12} molecules cm^{-3}, there is insignificant flux through this step on the 0.1 s time scale of our experiment. However, higher oxygen concentrations or faster rate constants can alter this conclusion. For instance, the similar mechanism following hydroxyl addition to ethene does lead to significant OH radical generation in our experiment. For ethene, (R6) is replaced by

$$RO \rightarrow R{=}O + CH_2OH \quad \text{(R6a)}$$

$$CH_2OH + O_2 \rightarrow CH_2O + HO_2 \quad \text{(R6b)}$$

Both of these reactions are rapid. This alkene mechanism is the most likely source of the well-documented difficulties in obtaining clean OH + alkene kinetics (Abbatt and Anderson [1991], Yin and Lee [1992]). The clear signature of these regeneration mechanisms is a strongly curved decay plot (Figure 6c). The absence of such curvature for the reactions discussed here indicates the absence of significant OH regeneration in these studies.

Figure 9 includes our own data and data from A90, obtained on the same HPF system though analyzed with slightly different methods. In addition, almost all other absolute measurements of this reaction (at room temperature) are shown. Our data, on average, fall slightly above that of A90. However, a point for point inspection (recognizing that they used a pitot tube for all velocity measurements) reveals that there is very little systematic

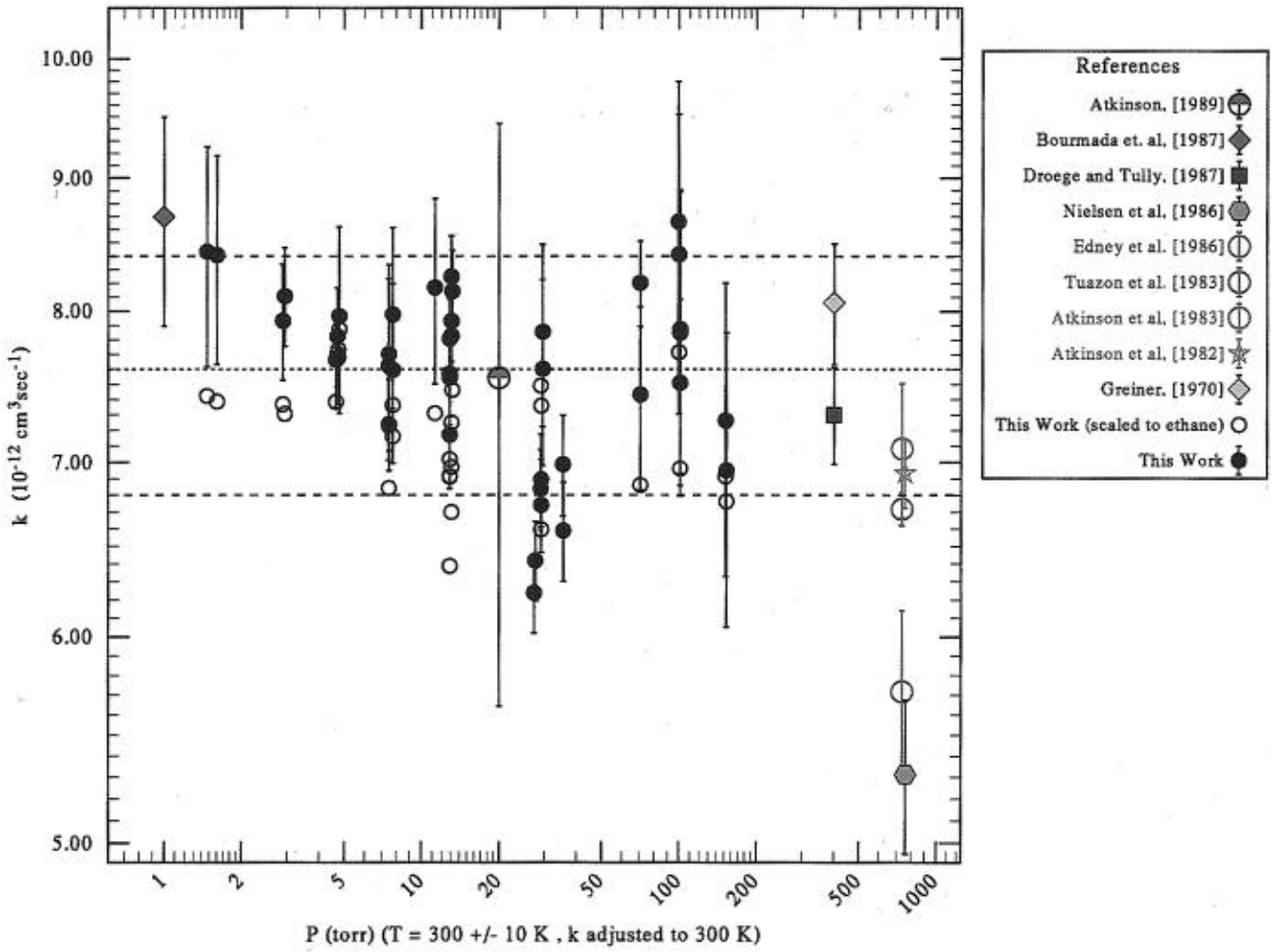

Figure 10. Diffusion-corrected rate constants for OH + cyclohexane. Our best estimate rate constant ($(7.6 \pm 0.8) \times 10^{-12}$ cm^3 molecules^{-1} s^{-1}) is shown as a horizontal dashed line, along with 95% confidence limits. Data from other published studies are shown with the symbols indicated in the legend. All values are corrected to 300 K.

difference between the data sets. While A90 did not include an explicit diffusion correction, they did apply a full two-dimensional inversion of radical data and the continuity equation to obtain most of their values; these are generally the data points with the larger estimated errors. Though they found no systematic difference between the continuity equation inversions and the simplified method of analyzing slopes along the spine of the radical plume, their data were obtained almost entirely under conditions where we find the correction to be small.

A simple averaging of our data would not be meaningful, as much of the residual variation still appears to be a systematic function of pressure, so the average value would be biased to the pressure with the most data points and/or the highest experimental precision. We therefore estimate the 300 K rate constant for OH + ethane to be $(2.55 \pm 0.3) \times 10^{-13}$ cm^3 molecules^{-1} s^{-1} at the 95% confidence level. This range includes nearly all of our observations as well as most other published values and includes all suspected sources of systematic error.

The overall agreement among the various studies is outstanding; a total of 17 studies form a group whose total range is 20% of the mean, while 11 studies, including ours, form a tighter cluster whose total range is 10%. Considering the complete dataset, we recommend a 300 K rate constant of $(2.55 \pm 0.15) \times 10^{-13}$ cm^3 molecules^{-1} s^{-1}, which includes 10 of the published rate constants.

Figure 10 includes much of the data available for the room temperature rate of the cyclohexane + OH reaction. Absolute measurements are shown as solid symbols in this figure, while relative measurements are shown as open symbols. In all cases, we have used the best current estimates of the calibration reaction rate constants when plotting the relative measurements. As in our earlier presentation, the open circles are the ratios of corresponding OH + cyclohexane and OH + ethane rate measurements, scaled to an assumed 300 K rate of OH + ethane of 2.45×10^{-13} cm^3 molecules^{-1} s^{-1}. Based on our measurements alone, we estimate the 300 K rate constant to be $(7.6 \pm 0.8) \times 10^{-12}$ cm^3 molecules^{-1} s^{-1} at the 95% confidence level. We also estimate a ratio k_1/k_2 of 29 ± 2.

The agreement with the literature is again good, though there is more scatter in the literature values. Interestingly, all of the published absolute values are paired either directly or closely with a measurement of the OH + ethane rate constant. The data of Greiner [1970] are too scattered to be meaningful. Both measurements by Nielsen et al. [1986] appear to fall outside the likely limits of the actual rate constants, but in opposite directions, so the ratio of the two rate constants is 17. The ethane rate constant of Tully et al. [1986] and the cyclohexane rate constant of Droege and Tully [1987] both agree with our values to within 5%, as does the ratio of 27.9. Both of the rate constants reported by Bourmada et al. [1987] are roughly 15% higher than our values, but the ratio of their two rate constants, 29.8, agrees with ours to within 3%; we attribute the slightly high values of Bourmada et al. [1987] to an error in velocity measurement common to both rate constant measurements.

Effects of Radial Asymmetry. Our model of kinetics in a diffusive flow only applies to radially symmetric plumes. Though we make every effort to configure the system symmetrically, completely symmetric plumes and velocity profiles can never be obtained, and the model gives no insight into the magnitude of any error introduced by asymmetries in our system. In order to assess the magnitude of this asymmetry effect, we conducted a series of measurements on intentionally asymmetric plumes. Runs were carried out under both laminar and turbulent conditions. The effects of asymmetry should be most pronounced in the laminar case because of the more highly curved velocity profile. Data were obtained for both reactions under study with plumes whose Gaussian centers were at a radius of 0 cm (much like that shown in Figure 3), 1 and 2 cm. In all cases the velocity and the OH radicals were measured in the core of the flow, at $r = 0$ cm. Results with the radical plume at 0 and 1 cm were entirely consistent with the data already presented. With the plume center at 2 cm radical count rates were quite low, so the resulting kinetic data was of poorer quality. The derived reaction rate constants differed by approximately 5% from the nominal value, with results for ethane higher than nominal and those for cyclohexane lower than nominal. It is most likely that these differences were caused by the reduced data quality and not by a systematic asymmetry effect, but such an effect (at the 5% level) cannot be ruled out for plumes 2 cm off center. However, radical plume centers can routinely be kept to well within 1 cm of the tube center, where there is no evidence for an asymmetry effect; we therefore conclude that the unmodeled effects of radial asymmetry contribute well under 5% to the overall uncertainty of our measurements.

Systematic Errors. There are four major sources of systematic error in the current high-pressure flow system: uncertain velocity measurements, secondary chemistry (either extra OH removal from reactive byproducts or OH regeneration from multistage processes), uncertainties in the absolute excess reagent concentration, and uncertainties in the diffusion correction. We shall deal with each in turn.

Our current velocity measurements, while based on first principles, require measurement of very small pressure gradients (10^{-3} Torr), often at very low system pressures. Tiny leaks, or very small effusion fluxes off of tubing walls, or very slow drifts in system pressure, can all cause systematic offsets in these measurements. Fortunately, the techniques we employ (pitot tubes, pressure head measurements, and single-pass mass flow measurements) are quite complementary. As we discussed earlier, we can achieve roughly 5% agreement between the methods under laminar conditions at moderate (7−10 Torr) pressures. At higher pressures, where the flow is generally turbulent, neither the gradient reading nor the bulk mass flow is simply related to the core velocity. However, the signal to noise of the pitot tube differential reading is much higher at high pressures, so the precision of the measurement is quite high. If the high signal to noise reflects accuracy no worse than that found under laminar conditions, the pitot tube based velocity readings in moderate Reynolds number turbulence are accurate. We therefore estimate the systematic error from the velocity measurements to be roughly 5% under all flow conditions when sufficient care has been taken to avoid biases caused by leakage or pressure drifts.

Secondary chemistry is the most active threat to accuracy. This is desirable. Secondary radical removal will be possible until we run the system with maximum radical concentrations of 10^{10} molecules cm^{-3} or less. Planned improvements in the laser system will accomplish this. At higher radical concentrations, careful studies of the effect of changing radical concentrations and various scrubber compounds must be combined with the primary rate measurements to ensure the overall accuracy. In our current system, where radical concentrations range from 10^{10} to 10^{11} molecules cm^{-3}, we cannot rigorously rule out a systematic bias (reaction rate constant too high) of roughly 10%, though the absence of changes in the calculated reaction rate constant at different initial radical concentrations suggests that this error is much smaller than 10%. Radical regeneration chemistry may persist at all radical concentrations, though it will benefit in two ways from increased sensitivity: radical sources run at lower fluxes will be much purer, and a wider dynamic range in the radical measurement will improve our ability to detect the upward curvature characteristic of regeneration.

The excess reagent measurement usually has very high signal to noise. Systematic errors come primarily from errors in reagent mixture preparation, reagent purity, or absorption cross sections. For most reagents we are able to prepare mixtures to roughly 1% accuracy. Reagent purity requirements depend on the speed of the primary reaction. In most cases establishing the purity of the reagent is not difficult; in some cases it is the major issue. We use the 184.9 nm (Hg line) F12 absorption cross section from JPL [1994] (121×10^{-20} cm^2). We have also measured this cross section on our system, obtaining the same result to within 1%. We therefore estimate the overall uncertainty in the excess reagent measurement to be at most 5% for all stable reagents. Reagents that react on the flow tube wall present a greater challenge, both because their cross sections are harder to establish and because the assumption of homogeneity in the excess reagent concentration throughout the reaction zone becomes less firm.

The diffusion correction developed in this work certainly is not highly accurate; however, it clearly removes a great deal of variance in the data presented. We estimate that the correction factor itself is uncertain by 30%. Fortunately, the correction only exceeds 30% below about 2 Torr system pressure, so the overall uncertainty due to axial diffusion or other unmodeled fluid dynamics is less than 5%, and usually lower still, over almost the entire operational range of the HPF system.

Taken in quadrature, these sources of systematic error combine to yield an overall accuracy in our derived reaction rate constants of between 10 and 15%. Because many of these errors affect all our observations identically, the accuracy to which we can derive the ratio of two reaction rate constants is much greater, lying between 5 and 10%.

Future Improvements. Each source of systematic error discussed previously is highly susceptible to being reduced through experimental refinements.

The velocity measurements are near their accuracy limits with the current techniques; however, laser doppler anemometry (LDA, Drain [1980]) is extremely accurate and can be easily adapted to our system. The primary challenge will be seeding our experiment with roughly 1 μm water droplets or ice particles for the measurement; however, a particle injector will bear a strong resemblance to our radical injector, so this is not expected to be troubling. Because the flow must be seeded for the LDA measurement, LDA will serve primarily as a calibration method for our other velocity measurements. However, those other methods are highly precise and the fluid dynamics in our system are very stable. We therefore anticipate being able to reduce the systematic uncertainty of our velocity measurements to roughly 2% over the entire operational range.

Our radical sensitivity can be improved in four ways: by multipassing the laser pulses in each detection axis, by increasing

the speed of the collection optics, by increasing laser power, and by reducing background scatter with improved baffling. By working on each we expect to increase the sensitivity of our OH detection by at least 2 orders of magnitude. This will allow us to operate under conditions where secondary reactions are far less likely. It will also allow operation in an atmosphere of air, where sensitivity is greatly reduced because of quenching.

Increased accuracy in excess reagent measurement requires only careful analytical work. We are currently engaged in an exhaustive set of measurements designed to permit highly accurate determinations of absorption cross sections for all reagents.

Conclusions. We are now able to measure radical molecule reactions to 10% or better accuracy. The major sources of uncertainty also appear to be vulnerable to further constraint; in particular, increased radical detection sensitivity and improved velocity measurements promise to greatly reduce the two major sources of error: secondary chemistry and uncertain velocities. Specific detection of reagents by IR absorption also promises to reduce our uncertainty. We therefore feel that a goal of 5% accuracy in these cases is realistic.

We have measured a great many radical−molecule reactions at elevated temperatures (Abbatt and Anderson [1991], Donahue et al. [1995b, in preparation], Mohrschladt et al. [1995b, in preparation]), as well as pressure-dependent reactions over a very wide pressure range (Donahue et al. [1995a], Mohrschladt et al. [1995a, in preparation]). These reactions range in speed from almost gas kinetic (i.e., OH + isoprene) to some of the slowest reactions measured in a flow tube (i.e., OH + D_2O, Dubey et al. [1995, in preparation]), a range in reactivity of more than 6 orders of magnitude. Work to modify the experiment to operate at subambient temperatures is proceeding. This shows great promise because of the wall-less nature of the system. While the accuracy in some of these cases is poorer than the tight limit presented here, in all cases the prospects for high accuracy are great.

In short, we are well on the way toward our goal of constructing a flow system capable of running under all conditions found in the atmosphere, and capable of producing reaction rate constant measurements with verifiably high accuracy. These measurements will not only greatly improve the kinetics database for interpretation of in-situ observations, they shall provide much tighter constraints in our effort to understand potential energy surfaces near transition states and reactive intermediate species.

Acknowledgment. We thank Ralf Mohrschladt, Manvendra Dubey, and Michele Sprengnether for stimulating discussions and helpful comments during the preparation of this manuscript. We also thank Noreen McDonald for help with the initial calculations of average core velocities, Ed Dunlea for experimental help, Dalia Trachtenberg for help with cross section measurements, and Paul Voss for research into the LDA technique. Data analysis would have been nearly impossible without the data acquisition system and software developed by the electrical engineers and computer programmers of the Atmospheric Research Project, particularly Norton Allen and Joe Demuz. This work was supported by NSF grant 8921312 to Harvard University, the DOE Global Change Distinguished Postdoctoral Fellowship Program, the Empire State Electrical Energy Research Corp. (ESEERCO), and the Electric Power Research Institute (EPRI).

References and Notes

Abbatt, J. P. D.; Demerjian, K. L.; Anderson, J. G. A new approach to free-radical kinetics: radially and axially resolved high-pressure discharge flow with results for OH + (C_2H_6, C_3H_8, *n*-C_4H_{10}, *n*-C_5H_{12}) → products at 297 K. *J. Phys. Chem.* **1990**, *94*, 4566.

Abbatt, J. P. D.; Anderson, J. G. High-pressure discharge flow kinetics and frontier orbital mechanistic analysis for OH + CH_2CCl_2, *cis*-CHClCHCl, *trans*-CHClCHCl, $CFClCF_2$, and CF_2CCl_2 → products. *J. Phys. Chem.* **1991**, *95*, 2382.

Atkinson, R.; Aschmann, S. M.; Winer, A. M.; Pitts, Jr., J. N. Rate constants for the reaction of OH radicals with a series of alkanes and alkenes at 299 ± 2 K. *Int. J. Chem. Kinet.* **1982**, *14*, 507.

Atkinson, R.; Aschmann, S. M.; Pitts, Jr., J. N. *Int. J. Chem. Kinet.* **1983**, *15*, 75.

Atkinson, R. Kinetics and mechanisms of the gas-phase reactions of the hydroxyl radical with organic compounds. *J. Phys. Chem. Ref. Data* **1989**, Monograph 1, 246 pp.

Atkinson, R.; Baulch, D. L.; Cox, R. A.; Hampson, Jr., R. F.; Kerr, J. A.; Troe, J. Evaluated kinetic and photochemical data for atmospheric chemistry: supplement III. *J. Phys. Chem. Ref. Data* **1989**, *18*, 881.

Batchelor, G. K. *An Introduction to Fluid Dynamics*; Cambridge University Press: London, 1967; 615 pp.

Baulch, D. L.; Campbell, I. M.; Saunders, S. M. Rate constants for the reactions of hydroxyl radicals with propane and ethane. *J. Chem. Soc., Faraday Trans.* **1985**, *81*, 259.

Bourmada, N.; Lafage, C.; Devolder, P. Absolute rate constants of the reactions of OH with cyclohexane and ethane at 296 ± 2 K by the discharge flow method. *Chem. Phys. Lett.* **1987**, *136*, 209.

Cohen, R. C., et al. Are models of catalytic removal of O_3 by HO_x accurate? Constraints from in situ measurements of the OH to HO_2 ratio. *Geophys. Res. Lett.* **1994**, *21*, 2539.

Devolder, P.; Carlier, M.; Pauwels, J. F.; Sochet, L. R. Rate constants for the reaction of OH with nitric acid: A new investigation by discharge flow resonance fluorescence. *Chem. Phys. Lett.* **1984**, *111*, 94.

Dobe, S.; Turanyi, T.; Iogansen, A. A.; Berces, T. Rate constants of the reactions of OH radicals with cyclopropane and cyclobutane. *Int. J. Chem. Kinet.* **1991**, *22*, 191.

Donahue, N. M.; Mohrschladt, R.; Dubey, M. K.; Demerjian, K. L.; Anderson, J. G. A High Pressure Flow Study of the Reaction OH + NO_2 → $HONO_2$ in Nitrogen. *J. Geophys. Res.*, submitted for publication.

Donahue, M.; Bell, K.; Demerjian, K. L.; Anderson, J. G. Temperature dependence of 11 OH + hydrocarbon abstraction reactions from 300 to 400 K. Manuscript in preparation.

Drain, L. E. *The Laser Doppler Technique*; John Wiley and Sons: New York, 1980; 430 pp.

Droege, A. T.; Tully, F. P. Hydrogen-atom abstraction from alkanes by OH. 6. Cyclopentane and cyclohexane. *J. Phys. Chem.* **1987**, *91*, 1222.

Dubey, M. K.; Mohrschladt, R.; Donahue, N. M.; Anderson, J. G. Testing theories of radical molecule reactivity with the isotopic scrambling reactions (^{18}OH, OD) + H_2O → products. Manuscript in preparation.

Edney, E. O.; Kleindienst, T. E.; Corse, E. W. *Int. J. Chem. Kinet.* **1986**, *18*, 1355.

Greiner, N. R. Hydroxyl radical kinetics by kinetic spectroscopy. VI. Reactions with alkanes in the range 300−500 K. *J. Chem. Phys.* **1970**, *53*, 1070.

Hinze, J. O. *Turbulence*; McGraw-Hill: New York, 1975; 790 pp.

Howard, C. J.; Evenson, K. M. Rate constants for the reactions of OH with ethane and some halogen substituted ethanes at 296 K. *J. Chem. Phys.* **1976**, *64*, 4303.

Howard, C. J. Kinetic measurements using flow tubes. *J. Phys. Chem.* **1979**, *83*, 3.

Jeong, K.; Hsu, J.; Jeffries, J. B.; Kaufman, F. Kinetics of the reactions of OH with C2H6, CH3CCl3, CH2ClCHCl2, CH2ClCClF2 and CH2FCF3. *J. Phys. Chem.* **1984**, *88*, 1222.

Kaufman, F. Kinetics of elementary radical reactions in the gas phase. *J. Phys. Chem.* **1984**, *88*, 4909.

Keyser, L. F. High-pressure flow kinetics. A study of the OH + HCl reaction from 2 to 100 Torr. *J. Phys. Chem.* **1984**, *88*, 4750.

Lee, J. H.; Tang, I. N. Absolute rate constants for the hydroxyl radical reactions with ethane, furan, and thiophene at room temperature. *J. Chem. Phys.* **1982**, *77*, 4459.

Leu, M. T. Rate constant for the reaction HO_2 + NO → OH + NO_2. *J. Chem. Phys.* **1979**, *70*, 1662.

Logan, J. A.; Prather, M. J.; Wofsy, S. C.; McElroy, M. B. Tropospheric chemistry: A global perspective; *J. Geophys. Res.* **1981**, *86*, 7210.

Mohrschladt, R.; Dubey, M. K.; Donahue, N. M.; Anderson, J. G. Kinetics and mechanism of the reaction ^{18}OH + NO_2 → products. Manuscript in preparation.

Mohrschladt, R.; Dubey, M. K.; Donahue, N. M.; Anderson, J. G. Temperature dependencies of the reactions (^{18}OH, OD) + H_2O → products. Manuscript in preparation.

Nielsen, O. J.; Munk, J.; Pagsberg, P.; Sillesen, A. Absolute rate constants for the gas phase reaction of OH radicals with cyclohexane and ethane at 295 K. *Chem. Phys. Lett.* **1986**, *128*, 168.

Overend, R. P.; Paraskevopoulos, G.; Cvetanovic, R. J. Rates of OH radical reactions. I. Reactions with H_2, CH_4, C_2H_6, and C_3H_8 at 295 K. *Can. J. Chem.* **1975**, *53*, 3374.

Schiffman, A.; Nelson, Jr., D. D.; Robinson, M. S.; Nesbitt, D. J. High resolution infrared flash kinetic spectroscopy of OH radicals. *J. Geophys. Res.* **1991**, *95*, 2629.

Schmidt, V.; Zhu, G. Y.; Becker, K. H.; Fink, E. H. Study of OH reactions at high pressures by excimer laser photolysis—dye laser fluorescence. *Ber. Bunsenges. Phys. Chem.* **1985**, *89*, 321.

Seeley, J. V.; Jayne, J. T.; Molina, M. J. High pressure fast-flow technique for gas phase kinetics studies. *Int. J. Chem. Kinet.* **1993**, *25*, 571.

Smith, C. A.; Molina, L. T.; Lamb, J. J.; Molina, M. J. Kinetics of the reaction of OH with pernitric and nitric acids. *Int. J. Chem. Kinet.* **1984**, *16*, 41.

Stachnik, R. A.; Molina, L. T.; Molina, M. J. Pressure and temperature dependencies of the reaction of OH with nitric acid. *J. Phys. Chem.* **1986**, *90*, 2777.

Stevens, P.; Anderson, J. *J. Phys. Chem.* **1992**, *96*, 1708.

Talukdar, R. K.; Mellouki, A.; Gierczak, T.; Barone, S.; Chiang, S-Y.; Ravishankara, A. R. Kinetics of the reactions of OH with alkanes. *J. Phys. Chem.* **1990**, *94*, 4566.

Toohey, D. W.; Anderson, J. G. Theoretical investigations of reactions of some radicals with HO_2. 1. Hydrogen abstractions by direct mechanisms. *J. Phys. Chem.* **1989**, *93*, 1049.

Tuazon, E. C.; Carter, W. P. L.; Atkinson, R.; Pitts, Jr., J. N. *Int. J. Chem. Kinet.* **1983**, *15*, 619.

Tully, F. P.; Ravishankara, A. R.; Carr, K. Kinetic study of the reactions of the hydroxyl radical with ethane and propane. *Int. J. Chem. Kinet.* **1983**, *15*, 1111.

Tully, F. P.; Droege, A. T.; Koszykowski, M. L.; Melius, C. F. Hydrogen-atom abstraction from alkanes by OH. 2. Ethane. *J. Phys. Chem.* **1986**, *90*, 691.

Vaghjiani, G. L.; Ravishankara, A. R. New measurement of the rate coefficient for the reaction of OH with methane. *Nature* **1991**, *350*, 406.

Wallington, T. J.; Neuman, D. M.; Kurylo, M. J. Kinetics of the gas phase reaction of hydroxyl radicals with ethane, benzene, and a series of halogenated benzenes over the temperature range 234−438 K. *Int. J. Chem. Kinet.* **1987**, *19*, 725.

Wennberg, P. O., et al. Aircraft-borne, laser-induced fluorescence instrument for the in situ detection of hydroxyl and hydroperoxyl radicals. *Rev. Sci. Instrum.* **1994**, *65*, 1858.

Wennberg, P. O., et al. Removal of stratospheric O_3 by radicals: In situ measurements of OH, HO_2, NO, NO_2, ClO, and BrO. *Science* **1994**, *266*, 398.

Westbrook, C. K.; Creighton, J.; Lund, C.; Dryer, F. L. A Numerical Model of Chemical Kinetics of Combustion in a Turbulent Flow Reactor. *J. Phys. Chem.* **1977**, *81*, 2542.

JP9525503